"Missing links" for the long-lived Macdonald and Arago hotspots, South Pacific Ocean

L Buff, M G Jackson, K Konrad, J G Konter, M. Bizimis, A Price, Estelle F. Rose-Koga, J. Blusztajn, A. A. P. Koppers

Publisher: GSA
Journal: GEOL: Geology
DOI:10.1130/G48276.1

"Missing links" for the long-lived Macdonald and Arago hotspots, South Pacific Ocean

L. Buff[1,*], M.G. Jackson[1], K. Konrad[2,3], J.G. Konter[4], M. Bizimis[5], A. Price[1], E.F. Rose-Koga[6], J. Blusztajn[7], and A.A.P. Koppers[3]

[1]*Department of Earth Science, University of California, Santa Barbara, California 93106, USA*

[2]*Department of Geoscience, University of Nevada, Las Vegas, Nevada 89154, USA*

[3]*Department of Geology and Geophysics, School of Ocean and Earth Science and Technology, University of Hawaii–Manoa, Honolulu, Hawaii 96822, USA*

[4]**[[Department?]]***University of Hawaii–Manoa, Honolulu, Hawaii 96822, USA*

[5]**[[Department?]]***University of South Carolina, Columbia, South Carolina 29208, USA*

[6]*Laboratoire Magmas et Volcans, Université Clermont Auvergne, CNRS-IRD-OPGC, F-63000 Clermont-Ferrand, France*

[7]*Department of Marine Chemistry, Woods Hole Oceanographic Institution, Woods Hole, Massachusetts 02543, USA*

*E-mail: lbuff@ucsb.edu

ABSTRACT

The Cook-Austral volcanic lineament extends from Macdonald Seamount (east) to Aitutaki Island (west) in the South Pacific Ocean and consists of hotspot-related volcanic islands, seamounts, and atolls. The Cook-Australs **[[lineament, or chain? Or Cook and Austal Islands?]]** have been characterized as multiple overlapping, age-progressive hotspot tracks generated by at least two mantle plumes, including the Arago

Publisher: GSA
Journal: GEOL: Geology
DOI:10.1130/G48276.1

and Macdonald plumes, which have fed volcano construction for ~20 m.y. The Arago and Macdonald hotspot tracks are argued to have been active for at least 70 m.y. and to extend northwest of the Cook-Australs into the Cretaceous-aged Tuvalu-Gilbert and Tokelau Island chains, respectively. Large gaps in sampling exist along the predicted hotspot tracks, complicating efforts seeking to show that the Arago and Macdonald hotspots have been continuous, long-lived sources of hotspot volcanism back into the Cretaceous. We present new major- and trace-element concentrations and radiogenic isotopes for three seamounts (Moki, Malulu, Dino) and one atoll (Rose), and new clinopyroxene $^{40}Ar/^{39}Ar$ ages for Rose (24.81 ± 1.02 Ma) and Moki (44.53 ± 10.05 Ma). All volcanoes are located in the poorly sampled region between the younger Cook-Austral and the older, Cretaceous portions of the Arago and Macdonald hotspot tracks. Absolute plate motion modeling indicates that the Rose and Moki volcanoes lie on or near the reconstructed traces of the Arago and Macdonald hotspots, respectively, and the $^{40}Ar/^{39}Ar$ ages for Rose and Moki align with the predicted age progression for the Arago (Rose) and Macdonald (Moki) hotspots, thereby linking the younger Cook-Austral and older Cretaceous portions of the long-lived (>70 m.y.) Arago and Macdonald hotspot tracks.

[[Note: Geology uses Ma for dates and absolute ages, and m.y. for durations and intervals of time.]]

INTRODUCTION

Intraplate volcanism is thought to result from buoyantly upwelling mantle plumes that partially melt beneath a moving plate, thereby producing age-progressive “hotspot” volcanism (e.g., Morgan, 1971). Some plume-derived volcanic chains, such as the

Publisher: GSA
Journal: GEOL: Geology
DOI:10.1130/G48276.1

Hawaii-Emperor and Louisville chains (North Pacific Ocean), are well defined with clear age progressions extending back to ca. 80 Ma (Sharp and Clague, 2006; Koppers et al., 2012; O'Connor et al., 2013). The Cook-Austral volcanic lineament in the South Pacific Ocean (hereafter Cook-Austral) is the manifestation of at least two overlapping hotspot tracks: the Arago (also referred to as "Rurutu" or "Atiu" trend) and Macdonald hotspot tracks. Denser sampling may reveal that not all seamounts along the predicted path of the Cook-Austral hotspots relate to these hotspots, but samples from two seamounts presented in this study strengthen hotspot age progressions anchored by young volcanism at Macdonald and Arago Seamounts, respectively (Fig. 1; Turner and Jarrard, 1982; Chauvel et al., 1997; Bonneville et al., 2002; Finlayson et al., 2018; Konrad et al., 2018; Rose and Koppers, 2019). While Cook-Austral volcanism has been argued to be relatively short-lived (0–20 m.y.; Chauvel et al., 1997; Lassiter et al., 2003), there is growing evidence that the mantle plumes responsible for Cook-Austral volcanism are long-lived features responsible for generating Pacific seamounts during the Cretaceous (Staudigel et al., 1991; Koppers et al., 2001, 2003, 2007; Konter et al., 2008; Finlayson et al., 2018; Konrad et al., 2018).

Using absolute plate motion models, Koppers et al. (2003, 2007) and Konter et al. (2008) showed that Cretaceous Pacific island chains, including the Tokelau and Tuvalu-Gilbert chains, were located over the Macdonald and Arago mantle plumes, respectively (Fig. 1). Konter et al. (2008) also showed geochemical similarities between the Cretaceous and Cook-Austral portions of these two hotspot tracks, strengthening the link between the younger and older segments of these hotspot tracks. Recently, Finlayson et al. (2018) and Konrad et al. (2018) showed that the Tuvalu chain captures the 50 Ma

"bend" (temporally and morphologically similar to the Hawaii-Emperor Bend) of the proposed Arago hotspot, thereby strengthening the link between the younger Cook-Austral and older Cretaceous segments of this proposed long-lived hotspot. However, volcanoes sampling the 45–10 Ma portion of the Arago hotspot represent an uncharacterized gap in the hotspot track. In contrast to the Arago hotspot, the Hawaii-Emperor Bend portion of the proposed Macdonald hotspot track has not yet been identified, and it will be important for linking the more recent Cook-Austral and older Cretaceous Tokelau segments of this hotspot track. Thus, while there is growing evidence that the Macdonald and Arago hotspots have been active since at least ca. 70 Ma, critical gaps in sampling and characterization of these two hotspot tracks weaken the hypothesis for long-lived, continuous volcanism.

Volcanoes in the region of the Samoan hotspot track, located ~1000 km west-northwest of Aitutaki Island, were found to exhibit geochemical signatures inconsistent with nearby Samoan volcanoes (Jackson et al., 2010). Termed "interlopers" (i.e., not belonging in the region; Jackson et al., 2010), these volcanoes (Rose Atoll and two seamounts, Malulu and Papatua) yielded samples exhibiting significant alteration and thick ferromanganese coatings, which contrast with the young, fresh lavas from Samoan volcanoes in the region. These interloper volcanoes also exhibit geochemical signatures consistent with an origin over Cook-Austral hotspots, which lie on, or close to, the reconstructed Macdonald and Arago hotspot traces.

We targeted the region between the Samoan hotspot and the Cook-Australs for additional sampling on the National Oceanic and Atmospheric Administration (NOAA) ocean exploration cruise EX1702 aboard the *Okeanos Explorer* in February–March 2017.

Publisher: GSA
Journal: GEOL: Geology
DOI:10.1130/G48276.1

Four volcanoes were sampled (Rose Atoll and Malulu, Moki, and Dino Seamounts) by remotely operated vehicle (ROV; Fig. 1; Tables S1 and S2 in the Supplemental Material[1]). Descriptions and thin section images are publicly available for all EX1702 samples used in this study (osu-mgr.org/noaa-ex1702). We present new Sr-Nd-Pb-Hf isotopic data (Fig. 2; Fig. S1) and major- and trace-element concentrations (Fig. S2) on these volcanoes. The new geochemical and geochronological data, in conjunction with previously published geochemical data for two legacy samples from Rose Atoll and one legacy sample each for Malulu and Papatua Seamounts (obtained by deep-sea dredging; see Supplemental Materials; Jackson et al., 2010), show that the Moki and Rose volcanoes provide "missing links" between the younger Cook-Austral and older Cretaceous segments of the Macdonald and Arago hotspots, respectively. These links extend the longevity of the Arago and Macdonald hotspots to at least 70 Ma, making them two of the longest-lived hotspots in the Pacific Ocean.

RESULTS AND DISCUSSION

Sample collection and analytical protocols for analysis of igneous material from Rose Atoll and the Malulu, Moki, and Dino Seamounts are detailed in the Supplemental Material. Due to the typically high degrees of submarine alteration, fine-grained to glass-rich groundmasses, and/or absence of traditionally dated phenocrystic phases (e.g., plagioclase), ages were not available for whole-rock samples from these five volcanoes; nonetheless, with extensive acid leaching, we could obtain radiogenic isotopic compositions on these samples (see the Supplemental Material). However, new advancements in $^{40}Ar/^{39}Ar$ methodology permit age determinations from clinopyroxene phenocrysts (Konrad et al., 2019). Using this technique, we successfully dated lava flows

Publisher: GSA
Journal: GEOL: Geology
DOI:10.1130/G48276.1

from the Moki and Rose volcanoes. The clinopyroxene separates from Rose Atoll (sample AVON2/3-D66–1) and Moki Seamount (sample EX1702-D7–2) both produced age spectra that met standard $^{40}Ar/^{39}Ar$ criteria, where plateaus included >60% of the $^{39}Ar_{(K)}$, and probability of fit (*P*) values were >5%. Two experiments for AVON2/3-D66–1, carried out on two clinopyroxene size fractions, produced concordant plateaus, which allowed the results to be combined and averaged (Fig. S3). The $^{40}Ar/^{36}Ar$ intercept values are within uncertainty of atmosphere (298.6), supporting the plateau age of 24.81 ± 1.02 Ma (2σ). This age places Rose Atoll squarely on the age progression for the Arago hotspot (Fig. 3), which is consistent with the observation that Rose Atoll is near the reconstructed trace of the Arago hotspot (Fig. 1). Sample EX1702-D7–2 contained low concentrations of potassium-derived ^{39}Ar and radiogenic ^{40}Ar, resulting in large uncertainties. The experiment produced a long plateau with a slightly higher-than-atmospheric $^{40}Ar/^{36}Ar$ intercept value of 313 ± 12 (2σ). Therefore, the inverse isochron age determination is preferred at 44.53 ± 10.05 Ma (2σ) (Fig. S3; Tables S3 and S4). While uncertainties are large, the Moki Seamount age places it on the Macdonald hotspot age progression (Fig. 3).

New geochemical data are presented in Tables S1 and S2. In radiogenic isotopic space, Macdonald and Arago Seamounts sampled HIMU (high μ = high $^{238}U/^{204}Pb$), enriched mantle (EM), and geochemically depleted end members (Chauvel et al., 1992, 1997; Lassiter et al., 2003; Hanyu et al., 2013) that may reflect a contribution from a common (C; Hanan and Graham, 1996) or FOZO (Hart et al., 1992) components (Konter et al., 2008; Fig. 2; Fig. S1). While Rose Atoll erupted over the Arago hotspot, whole-rock (Jackson et al., 2010) and glass geochemistry does not consistently plot in the fields

Publisher: GSA
Journal: GEOL: Geology
DOI:10.1130/G48276.1

for Arago hotspot volcanoes in the Cook-Austral volcanic lineament or the older portion of the Arago hotspot (Gilbert, Tuvalu, Marshall, and Wake islands and seamounts), and in some isotope spaces, one or multiple Rose samples plot only in the field for Macdonald hotspot volcanoes (Fig. 2; Fig. S1).

The Moki Seamount sample yielded an age with greater uncertainty, but the age is nonetheless consistent with a Macdonald hotspot origin, and the Moki sample consistently falls in a region of isotopic space that overlaps with Macdonald hotspot volcanoes (Fig. 2; Fig. S1). In the hotspot reconstruction using the Wessel and Kroenke (2008) absolute plate motion model, Moki plots significantly closer to the reconstructed trace of the Macdonald hotspot track than the Arago hotspot track, consistent with the geochronological and geochemical data provided here (Fig. 1). While uncertainties are large, the Moki Seamount age places it on the Macdonald hotspot age progression (Fig. 3), and the age for Moki overlaps with the reconstructed Macdonald hotspot track, even at the 1σ level.

The Dino Seamount sample and the new Malulu Seamount sample presented here (EX1702-D12–5) consistently plot in the field for Macdonald hotspot volcanoes in the Cook-Austral volcanic lineament, but age data are needed before a Macdonald hotspot designation can be assigned. Papatua Seamount (Jackson et al., 2010) plots in a region that overlaps the Macdonald and Arago hotspots in all isotopic spaces for which there are available data, except for the $^{206}Pb/^{204}Pb$ versus $^{143}Nd/^{144}Nd$ isotope space, where it plots in the Macdonald field (Fig. 2; Fig. S1). Unfortunately, Papatua is also geographically located on a portion of the reconstructed hotspot tracks where the Macdonald and Arago

tracks overlap, preventing a hotspot designation for Papatua. Age data are needed to determine the hotspot origin of this seamount.

The link between the younger Cook-Austral and older Cretaceous segments of the Macdonald and Arago hotspots provided by samples from Moki Seamount and Rose Atoll, respectively, has two key implications: (1) it allows us to posit, with greater confidence, that the Macdonald hotspot is both continuous and long-lived, and (2) it supports previous arguments for the longevity of the Arago hotspot (Finlayson et al., 2018). Thus, the Macdonald and Arago hotspots join Hawaii (Tarduno et al., 2003; O'Connor et al., 2013) and Louisville (Lonsdale, 1988; Koppers et al., 2012) as two Pacific hotspots for which activity has been mapped for least 70 m.y.

An important outcome of this work is the strengthening of the case for the longevity of the Arago and Macdonald hotspots. However, it is becoming increasingly clear that the Arago and Macdonald hotspots show significant overlap in Sr-Nd-Pb-Hf isotopic space, and it is the combination of geochemistry and ages that uniquely constrains the hotspot to which a given seamount belongs. For example, the Arago and Macdonald plumes have consistently sampled the most extreme HIMU compositions ($^{206}Pb/^{204}Pb$ up to 21.42 for Arago, and 21.93 for Macdonald; Fig. 2) in the Pacific since the Cretaceous (Konter et al., 2008; Hanyu et al., 2011; Finlayson et al., 2018). The reason for this may be due to the close proximity of the two hotspots: The long-lived Arago hotspot is located just ~1200 km west-northwest from the Macdonald hotspot. If both hotspots are fed by mantle plumes that emerge from the core-mantle boundary, the plume conduits are separated by only ~660 km at the core-mantle boundary. Thus, the regions (i.e., "feeding zones") at the core-mantle boundary that are sourcing material to

the upwelling Macdonald and Arago plumes may overlap, explaining the similar isotopic signatures at both hotspots (Fig. 2). If both plumes have been producing active volcanism for >70 m.y., an important dynamic question to be addressed is how the two closely spaced plume conduits have interacted over geologic time (Lassiter et al., 2003). Both plumes arise from the large low-shear-wave-velocity province (LLSVP) situated on top of the core-mantle boundary (CMB) beneath the Pacific (Jackson et al., 2018), and long-lived HIMU signatures in both plumes might suggest that this is a geochemical characteristic of the region of the Pacific LLSVP that is sourced by both plumes.

ACKNOWLEDGMENTS

We acknowledge helpful reviews from Oliver Nebel and two anonymous reviewers. We thank the National Oceanic and Atmospheric Administration (NOAA) Ocean Explorer program and the crew of the *Okeanos Explorer* expedition EX1702. The Oregon State University Marine and Geology Repository provided samples from the EX1702 expedition. Konrad thanks D. Heaton for assistance with the age determinations. Jackson acknowledges support from National Science Foundation grants OCE-1912931, EAR-1900652, and EAR-1429648. Rose-Koga acknowledges support from Laboratory of Excellence ClerVolc (Clermont-Ferrand Centre for Volcano Research). This is Laboratory of Excellence ClerVolc contribution 438.

REFERENCES CITED

Bonneville, A., Le Suave, R., Audin, L., Clouard, V., Dosso, L., Gillot, P.Y., Janney, P., and Maamaatuaiahutapu, K., 2002, Arago Seamount: The missing hotspot found in the Austral Islands: Geology, v. 30, p. 1023–1026, https://doi.org/10.1130/0091-7613(2002)030<1023:ASTMHF>2.0.CO;2.

206 Chauvel, C., Hofmann, A.W., and Vidal, P., 1992, HIMU-EM: The French Polynesian
207 connection: Earth and Planetary Science Letters, v. 110, p. 99–119,
208 https://doi.org/10.1016/0012-821X(92)90042-T.
209 Chauvel, C., McDonough, W., Guille, G., Maury, R., and Duncan, R., 1997, Contrasting
210 old and young volcanism in Rurutu Island, Austral chain: Chemical Geology, v. 139,
211 p. 125–143, https://doi.org/10.1016/S0009-2541(97)00029-6.
212 Finlayson, V., Konter, J.G., Konrad, K., Koppers, A.A.P., Jackson, M.G., and Rooney,
213 T.O., 2018, Sr-Pb-Nd-Hf isotopes and $^{40}Ar/^{39}Ar$ ages reveal a Hawaii-Emperor–style
214 bend in the Rurutu hotspot: Earth and Planetary Science Letters, v. 500, p. 168–179,
215 https://doi.org/10.1016/j.epsl.2018.08.020.
216 Hanan, B.B., and Graham, W.D., 1996, Lead and helium isotope evidence from oceanic
217 basalts for a common deep source of mantle plumes: Science, v. 272, p. 991–995,
218 https://doi.org/10.1126/science.272.5264.991.
219 Hanyu, T., Tatsumi, Y., Senda, R., Miyazaki, T., Chang, Q., Hirahara, Y., Takahashi, T.,
220 Kawabata, H., Suzuki, K., Kimura, J., Nakai, S., 2011, Geochemical characteristics
221 and origin of the HIMU reservoir: A possible mantle plume source in the lower
222 mantle: Geochemistry Geophysics Geosystems, v. 12, Q0AC09,
223 https://doi.org/10.1029/2010GC003252.
224 Hanyu, T., Dosso, L., Ishizuka, O., Tani, K., Hanan, B.B., Adam, C., Nakai, S., Senda,
225 R., Chang, Q., and Tatsumi, Y., 2013, Geochemical diversity in submarine HIMU
226 basalts from Austral Islands, French Polynesia: Contributions to Mineralogy and
227 Petrology, v. 166, p. 1285–1304, https://doi.org/10.1007/s00410-013-0926-x.

228 Hart, S.R., Hauri, E.H., Oschmann, L.A., and Whitehead, J.A., 1992, Mantle plumes and
229 entrainment: Isotopic evidence: Science, v. 256, p. 517–520,
230 https://doi.org/10.1126/science.256.5056.517.
231 Jackson, M.G., Hart, S.R., Konter, J.G., Koppers, A.A.P., Staudigel, H., Kurz, M.D.,
232 Blusztajn, J., and Sinton, J.M., 2010, The Samoan hotspot track on a "hotspot
233 highway": Implications for mantle plumes and a deep Samoan mantle source:
234 Geochemistry Geophysics Geosystems, v. 11, Q12009,
235 https://doi.org/10.1029/2010GC003232.
236 Jackson, M.G., Becker, T.W., and Konter, J.G., 2018, Geochemistry and distribution of
237 recycled domains in the mantle inferred from Nd and Pb isotopes in oceanic hot
238 spots: Implications for storage in the large low shear wave velocity provinces:
239 Geochemistry Geophysics Geosystems, v. 19, p. 3496–3519,
240 https://doi.org/10.1029/2018GC007552.
241 Jackson, M.G., Halldórsson, S.A., Price, A., Kurz, M.D., Konter, J.G., Koppers, A.A.P.,
242 Day, J.M.D., 2020, Contrasting old and young volcanism from Aitutaki, Cook
243 Islands: Implications for the origins of the Cook-Austral volcanic chain: Journal of
244 Petrology, v. 61, no. 3, p. egaa037, https://doi.org/10.1093/petrology/egaa037.
245 Konrad, K., Koppers, A.A.P., Steinberger, B., Finlayson, V., Konter, J., and Jackson,
246 M.G., 2018, On the relative motions of long-lived Pacific mantle plumes: Nature
247 Communications, v. 9, p. 854, https://doi.org/10.1038/s41467-018-03277-x.
248 Konrad, K., Koppers, A.A., Balbas, A.M., Miggins, D.P., and Heaton, D.E., 2019, Dating
249 clinopyroxene phenocrysts in submarine basalts using $^{40}Ar/^{39}Ar$ geochronology:

Geochemistry Geophysics Geosystems, v. 20, p. 1041–1053, https://doi.org/10.1029/2018GC007697.

Konter, J.G., Hanan, B.B., Blichert-Toft, J., Koppers, A.A.P., Plank, T., and Staudigel, H., 2008, One hundred million years of mantle geochemical history suggest the retiring of mantle plumes is premature: Earth and Planetary Science Letters, v. 275, p. 285–295, https://doi.org/10.1016/j.epsl.2008.08.023.

Koppers, A.A.P., Phipps Morgan, J., and Staudigel, H., 2001, Testing the fixed hotspot hypothesis using $^{40}Ar/^{39}Ar$ age progressions along seamount trails: Earth and Planetary Science Letters, v. 185, p. 237–252, https://doi.org/10.1016/S0012-821X(00)00387-3.

Koppers, A.A.P., Pringle, M.S., and Wijbrans, J.R., 2003, Short-lived and discontinuous intraplate volcanism in the South Pacific: Hot spots or extensional volcanism?: Geochemistry Geophysics Geosystems, v. 4, 1089, https://doi.org/10.1029/2003GC000533.

Koppers, A.A.P., Staudigel, H., Phipps Morgan, J., and Duncan, R.A., 2007, Nonlinear $^{40}Ar/^{39}Ar$ age systematics along the Gilbert Ridge and Tokelau Seamount trail and the timing of the Hawaii-Emperor Bend: Geochemistry Geophysics Geosystems, v. 8, Q06L13, https://doi.org/10.1029/2006GC001489.

Koppers, A.A.P., et al., 2012, Limited latitudinal mantle plume motion for the Louisville hotspot: Nature Geoscience, v. 5, p. 911–917, https://doi.org/10.1038/ngeo1638.

Lassiter, J.C., Blichert-Toft, J., Hauri, E.H., and Barsczus, H.G., 2003, Isotope and trace element variations in lavas from Raivavae and Rapa, Cook–Austral islands: Constraints on the nature of HIMU- and EM-mantle and the origin of mid-plate

volcanism in French Polynesia: Chemical Geology, v. 202, p. 115–138, https://doi.org/10.1016/j.chemgeo.2003.08.002.

Lonsdale, P., 1988, Geography and history of the Louisville hotspot chain in the southwest Pacific: Journal of Geophysical Research, v. 93, p. 3078–3104, https://doi.org/10.1029/JB093iB04p03078.

Morgan, W.J., 1971, Convection plumes in the lower mantle: Nature, v. 230, p. 42–43, https://doi.org/10.1038/230042a0.

O'Connor, J.M., Steinberger, B., Regelous, M., Koppers, A.A.P., Wijbrans, J.R., Haase, K.M., Stoffers, P., Jokat, W., and Garbe-Schönberg, D., 2013, Constraints on past plate and mantle motion from new ages for the Hawaiian-Emperor Seamount Chain: Geochemistry Geophysics Geosystems, v. 14, p. 4564–4584, https://doi.org/10.1002/ggge.20267.

Rose, J., and Koppers, A.A.P., 2019, Simplifying age progressions within the Cook-Austral Islands using high-resolution ARGUS-VI $^{40}Ar/^{39}Ar$ incremental heating ages: Geochemistry Geophysics Geosystems, v. 20, p. 4756–4778, https://doi.org/10.1029/2019GC008302.

Sharp, W.D., and Clague, D.A., 2006, 50-Ma initiation of Hawaiian-Emperor Bend records major change in Pacific plate motion: Science, v. 313, p. 1281–1284, https://doi.org/10.1126/science.1128489.

Staudigel, H., Park, K.-H., Pringle, M., Rubenstone, J.L., Smith, W.H.F., and Zindler, A., 1991, The longevity of the South Pacific isotopic and thermal anomaly: Earth and Planetary Science Letters, v. 102, p. 24–44, https://doi.org/10.1016/0012-821X(91)90015-A.

Tarduno, J.A., Duncan, R.A., Scholl, D.W., Cottrell, R.D., Steinberger, B., Thordarson, T., Kerr, B.C., Neal, C.R., Frey, F.A., Torii, M., and Carvallo, C., 2003, The Emperor Seamounts: Southward motion of the Hawaiian hotspot plume in Earth's mantle: Science, v. 301, p. 1064–1069, https://doi.org/10.1126/science.1086442.

Turner, D.L., and Jarrard, R.D., 1982, K/Ar dating of the Cook Austral island chain; a test of the hot spot hypothesis: Journal of Volcanology and Geothermal Research, v. 12, p. 187–220, https://doi.org/10.1016/0377-0273(82)90027-0.

Wessel, P., and Kroenke, L.W., 2008, Pacific absolute plate motion since 145 Ma: An assessment of the fixed hot spot hypothesis: Journal of Geophysical Research, v. 113, B06101, https://doi.org/10.1029/2007JB005499.

FIGURE CAPTIONS

Figure 1. Map of current Cook-Austral, Tokelau, and Tuvalu-Gilbert Seamounts and volcanoes (South Pacific Ocean) pertaining to this study, showing reconstructed tracks for Samoan and Cook-Austral hotspots (including Macdonald and Arago hotspots). Shaded bands anchored to active portions of each hotspot track are reconstructed traces for each hotspot track (dark blue—Macdonald, red—Arago, yellow—Rarotonga, purple—Samoa) and are based on the absolute plate motion model of Wessel and Kroenke (2008); stars mark proposed hotspot locations. Blue circles represent volcanoes previously associated with the Macdonald hotspot, and red circles represent volcanoes previously associated with the Arago hotspot (data sources: Koppers et al., 2007; Konrad et al., 2018; Rose and Koppers, 2019; Jackson et al., 2020). Five interloper volcanoes investigated in this study are also indicated on this map: Moki, Malulu, Rose, Dino, and Papatua.

Publisher: GSA
Journal: GEOL: Geology
DOI:10.1130/G48276.1

Figure 2. $^{143}Nd/^{144}Nd$ vs. $^{206}Pb/^{204}Pb$ for volcanoes in this study plotted with existing data from Macdonald and Arago hotspot-related volcanoes (South Pacific Ocean). Moki and Malulu isotopic data produced for this study are from clinopyroxene phenocrysts, as seawater alteration prevented analysis of whole-rock samples. New data also include pillow rim glass analyses from Rose Atoll, whole-rock data from Dino Seamount, and whole-rock data from Rose, Malulu, and Papatua lavas previously published by Jackson et al. (2010). Younger portions of the Arago (red field) and Macdonald (blue) hotspots in the Cook-Austral volcanic lineament are distinguished from older portions of these hotspots (light gray with long dashed lines for Tuvalu, Gilbert, Marshall, and Wake islands and seamounts [i.e., Old Arago]; dark gray with short dashed lines for Tokelau Islands and seamounts [i.e., Old Macdonald]). Age-corrected (to time of eruption) isotopic values are shown, but only where ages are available (Moki Seamount and Rose Atoll). Three undated Rose Atoll samples are assumed to have same age as sample EX1702-D3–2. Isotopic shift due to age correction is shown by line extending from respective data points (representing magnitude and direction of age correction). Other samples (Malulu, Papatua, and Dino) are not associated with ages, and age corrections are not provided. All data not produced in this study were previously published and downloaded from the Georoc database (http://georoc.mpch681mainz.gwdg.de/georoc). HIMU—high μ = high $^{238}U/^{204}Pb$; EM1–EM2—enriched mantle sources. Figure is modified after Jackson et al. (2020).

Publisher: GSA
Journal: GEOL: Geology
DOI:10.1130/G48276.1

Figure 3. Hotspot track age-distance plot showing Rose and Moki volcanoes (South Pacific Ocean), including volcanoes associated with Macdonald, Arago, Rarotonga, and Samoa trends plotted along their respective reconstructed hotspot track. Clinopyroxene incremental-heating $^{40}Ar/^{39}Ar$ ages for Rose and Moki are labeled (with 2σ uncertainties). Great circle distances from active hotspots were used. The absolute plate motion model of Wessel and Kroenke (2008), used to model volcanic age progressions, is shown for each hotspot (blue—Macdonald, red—Arago, black—Rarotonga, and pink—Samoa). Estimates for uncertainty in the Wessel and Kroenke (2008) model are also provided (dashed lines). Ages for Tokelau and Tuvalu-Gilbert volcanoes were published by Staudigel et al. (2001)**[[Staudigel et al. (2001) is not in the reference list.]]**, Konter et al. (2008), Finlayson et al. (2018), and Konrad et al. (2018). Ages for Cook-Austral volcanic lineament were compiled by Jackson et al. (2020) and Rose and Koppers (2019).

[1]Supplemental Material. **[[Please provide a brief caption here.]]**. Please visit https://doi.org/10.1130/XXXXX to access the supplemental material, and contact editing@geosociety.org with any questions.

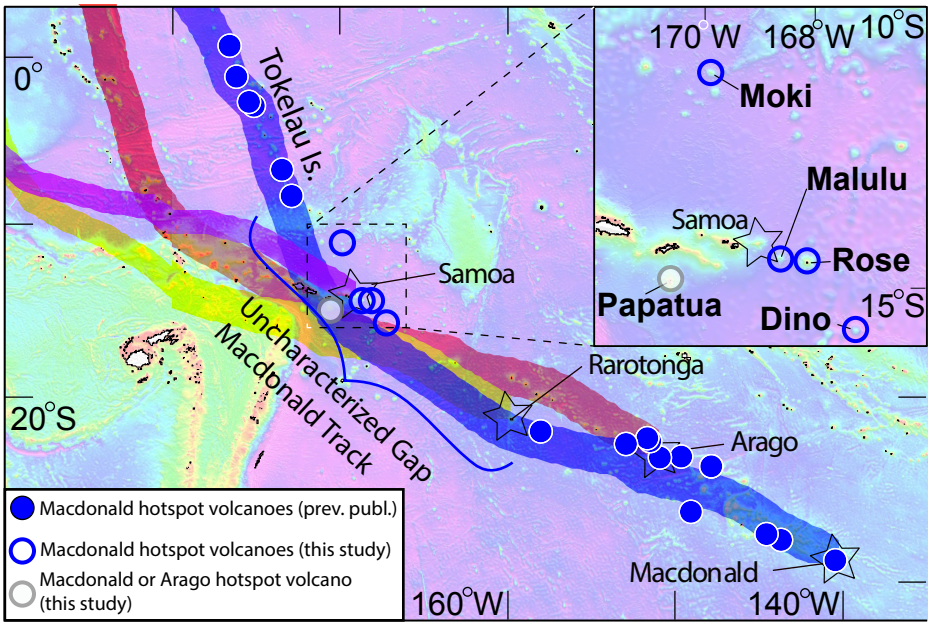
0°
20°S
160°W
140°W
170°W
168°W
10°S
15°S
Tokelau Is.
Samoa
Uncharacterized Gap
Macdonald Track
Rarotonga
Arago
Macdonald
Moki
Malulu
Samoa
Rose
Papatua
Dino
Macdonald hotspot volcanoes (prev. publ.)
Macdonald hotspot volcanoes (this study)
Macdonald or Arago hotspot volcano (this study)

Figure 1

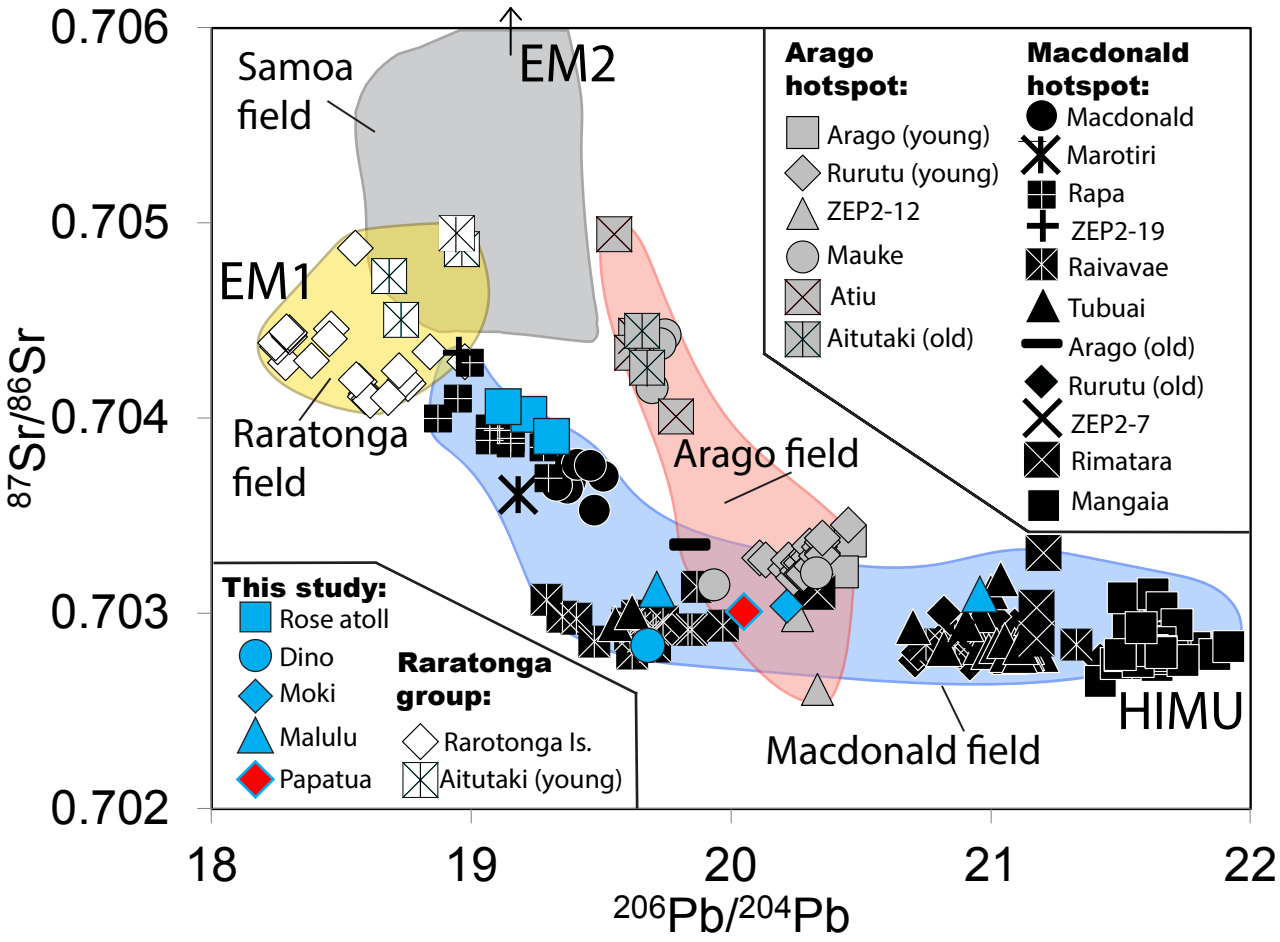
0.706
0.705
0.704
0.703
0.702
87Sr/86Sr
18
19
20
21
22
206Pb/204Pb
Samoa field
EM2
EM1
Raratonga field
Arago field
Macdonald field
HIMU
Arago hotspot:
Arago (young)
Rurutu (young)
ZEP2-12
Mauke
Atiu
Aitutaki (old)
Macdonald hotspot:
Macdonald
Marotiri
Rapa
ZEP2-19
Raivavae
Tubuai
Arago (old)
Rurutu (old)
ZEP2-7
Rimatara
Mangaia
This study:
Rose atoll
Dino
Moki
Malulu
Papatua
Raratonga group:
Rarotonga Is.
Aitutaki (young)

Figure 2

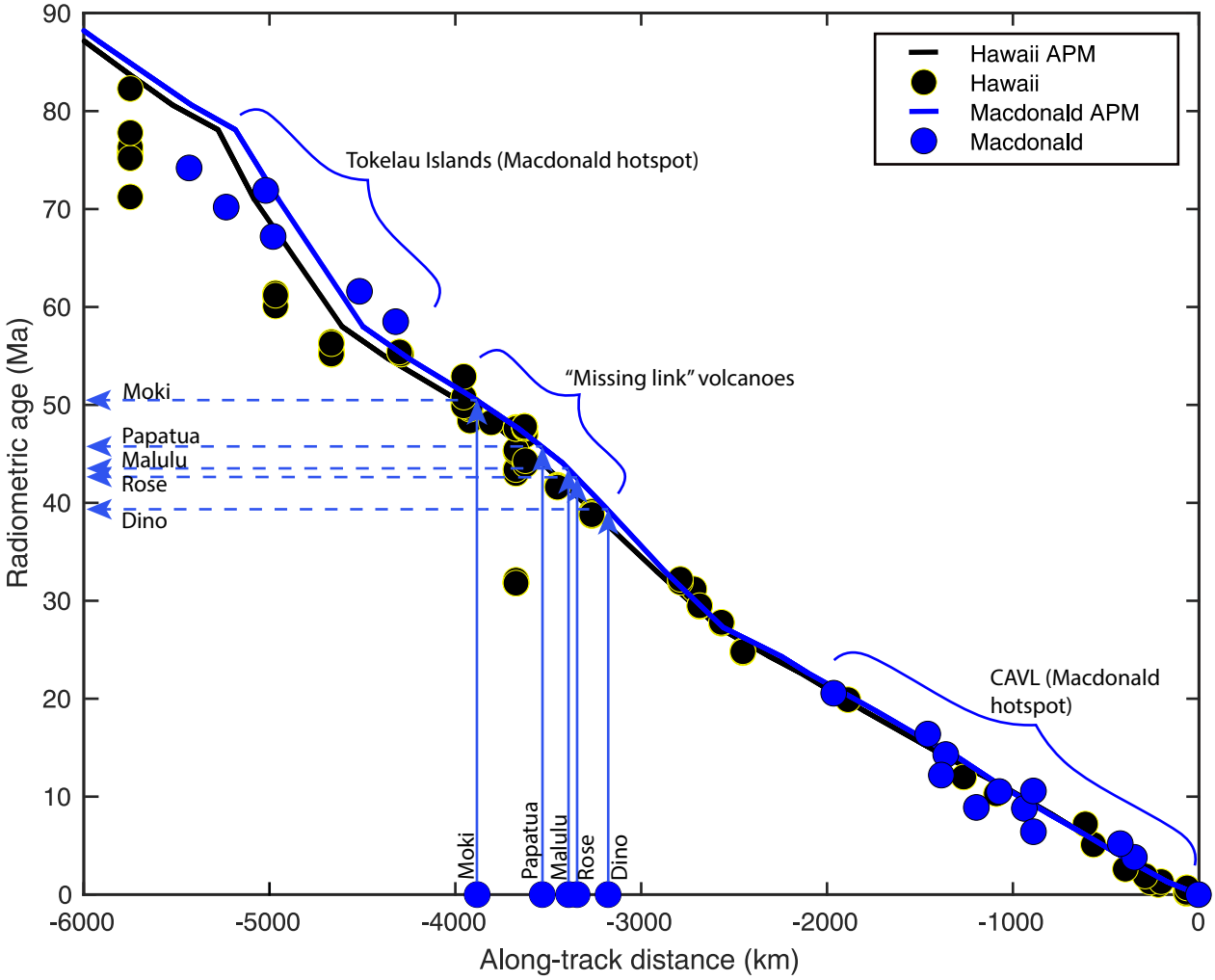
Hawaii APM
Hawaii
Macdonald APM
Macdonald
Tokelau Islands (Macdonald hotspot)
"Missing link" volcanoes
CAVL (Macdonald hotspot)
Moki
Papatua
Malulu
Rose
Dino
Radiometric age (Ma)
Along-track distance (km)
90
80
70
60
50
40
30
20
10
0
-6000
-5000
-4000
-3000
-2000
-1000
0

Figure 3

Supplemental Materials

Methods

Sample locations, preparation and wet chemistry.

The samples in this study were collected by deep submarine dredging from four seamounts (Papatua, Moki, Seamount D ["Dino"], Malulu) and one atoll (Rose) in the Samoan region. Several samples in this study were collected during the 2017 expedition (EX1702) aboard the NOAA *Okeanos Explorer*: Moki seamount (basaltic sample D7-2), Dino seamount (basaltic sample D11-1), Rose atoll (pillow fragment sample D3-2), and Malulu seamount (hyaloclastite sample D12-5). Finally, two samples from the 1999 AVON2/3 expedition aboard the R/V Melville which were previously characterized are presented here with modern Pb-isotopic analyses: AVON2/3-D67-11 from Malulu seamount which is an altered basalt, and basaltic sample AVON2/3-D66-1 from Rose atoll. Tables S1 and S2 present previously published data on these two Rose samples in addition to two other samples—AVON2/3-D65-18 (from Malulu seamount) and ALIA-DR129-05 (from Papatua seamount) —from non-Samoan seamounts in the Samoan region. Sample locations and geochemical characterization of these four previously published lavas can be found in **Jackson et al. (2010)**.

Samples were crushed in plastic bags to avoid exposure to metal. Crushed material was then sieved. For two samples (EX1702-D12-5 hyaloclastite from Malulu seamount and EX1702-D7-2 basalt from Moki seamount), clinopyroxene was removed for radiogenic isotopic work due to the lack of fresh basaltic material. For Rose atoll sample EX1702-D3-2, volcanic glass was removed from the pillow rim for radiogenic isotopic analysis (this glass was also characterized for major and trace element compositions, but we also present whole rock major and trace element data for this sample as well). For sample EX1702-11-1 (Seamount D), 200 mg of the freshest (0.5 to 1 mm) rock chips were analyzed, targeting groundmass. We also separated the freshest groundmass chips from two previously characterized lavas—AVON2/3-D66-1 (Rose atoll) and AVON2/3-D67-11 (Malulu seamount)—for a new characterization using modern Pb isotopic analyses and new analyses of Sr and Nd isotopes on the same material.

The groundmass samples (including the EX1702-D3-2 glass) were treated with a heavy leaching protocol described in **Price et al. (2016)** which, in addition to the 6N HCl leaching treatment, uses hot 4N HNO_3 and hot 30% H_2O_2. The clinopyroxene samples were first leached in concentrated HCl for 1 hour at 40º C, then in concentrated nitric for 1 hour at 40º C, with ~1 hour of sonication in the same acid following each leaching step; after this initial leach, the clinopyroxenes were subjected to the same "heavy leaching" as the groundmass and glass samples (and, following leaching, only pristine clinopyroxenes were selected for dissolution and analysis). Note that replicated analysis of the D11-1 groundmass followed additional leaching: it was treated with the strong leaching protocol followed by an additional 8 hours of leaching in 6N HCl at 60º C and an additional 10 minutes leaching in cold concentrated HF; this may explain the offset in Sr, Nd, and Pb isotopes between the original and replicate rounds of analyses of this sample. USGS reference materials were not leached. Following leaching, samples were rinsed and sonicated repeatedly in MilliQ H_2O ($\geq$ 18.2 MΩ · cm deionized water). Sample dissolution, wet chemistry (including Sr, Pb, Hf and Nd elemental separations), and mass spectrometry was carried out in one of the three following institutions:

1. One batch of samples underwent Sr, Nd, and Pb chemical separations at UCSB, with Sr and Nd isotopes analyzed on the UCSB TIMS and Pb isotopes analyzed on the WHOI

MC-ICP-MS; the wet chemistry follows methods developed in **Price et al. (2014)** with modifications as follows: Following dissolution in concentrated HF and HNO_3, Sr and Pb were purified by two passes through 100 μL of Eichrom Sr resin (25-50 μm), and Nd purified was purified from the wash of the Sr resin using a two-step method employing Eichrom TRU resin (100-150 μm) followed by Eichrom LN-Spec resin (50-100 μm). Total procedural blanks are <200 pg for Sr, <50 pg for Nd, and < 120 pg for Pb.

2. A second batch of samples underwent Sr, Nd, and Pb chemical separations at UCSB as described above, with Sr and Nd isotopes analyzed on the UCSB TIMS. However, Pb isotopes were analyzed on the University of South Carolina MC-ICP-MS.
3. A third batch of samples, which included just the cpx separates for EX1702-D12-5 and EX1702-D7-5, underwent dissolution, chemical separations (for Sr, Nd, Hf, and Pb), and mass spectrometry at the University of South Carolina.

Further description of wet chemistry and mass spectrometry is provided below.

Sr and Nd mass spectrometry at UCSB and Pb mass spectrometry at WHOI.

Sr and Nd isotopes were analyzed on a Thermo Triton Plus TIMS mass spectrometer housed at UCSB. 500 ng of Sr or Nd was loaded on outgassed, zone-refined Re (99.999% purity, H-Cross, USA) filaments. With the exception of the first $^{87}Sr/^{86}Sr$ analyses (EX1702-D12-5 clinopyroxene, EX1702-D7-5 clinopyroxene, EX1702-D11-1, EX1702-D3-2) and associated standards, which used a 33 picoamp gainboard but did not employ amplifier rotation, all other Sr and Nd isotopic analyses of samples, replicates, and associated standards employed amplifier rotation on 10^{11} ohm amplifiers and a 3.3 picoamp gainboard. Gains were run with the start of a new barrel. Approximately 20% of analysis time was devoted to baselines: baselines are taken with each rotation of the amplifiers (i.e., because 5 amplifiers-cup pairs were used during analyses, 5 baselines were taken during each full amplifier rotation). Intensities were kept at approximately 3V on mass 88 and 3V on mass 144 during $^{87}Sr/^{86}Sr$ and $^{143}Nd/^{144}Nd$ analyses, respectively. Sr and Nd isotopes were corrected for mass bias assuming an exponential law and using canonical $^{86}Sr/^{88}Sr$ and $^{146}Nd/^{144}Nd$ ratios of 0.1194 and 0.7219, respectively. Isobaric interferences from Rb and Sm were corrected by monitoring masses 85 and 147, but corrections to the $^{87}Sr/^{86}Sr$ and $^{143}Nd/^{144}Nd$ ratios were nominal. USGS reference materials (processed through all steps of wet chemistry and column chemistry with unknowns at UCSB) and sample unknowns were corrected for the offset between preferred and measured standard (NBS987 or JNdi) values with each barrel: preferred value for NBS987 $^{87}Sr/^{86}Sr$ is 0.710240, and JNdi is 0.512099 (**Garçon et al., 2018**). On the UCSB Triton Plus the average $^{87}Sr/^{86}Sr$ and $^{143}Nd/^{144}Nd$ and long-term reproducibility, up to and including this study, of NBS987 and JNdi using amplifier rotation is 0.710246 ± 0.000011 (2SD, *N*=29) and, 0.512100 ± 0.000004 (2SD, *N*=27), respectively. The corresponding average $^{87}Sr/^{86}Sr$ and long-term reproducibility when analyzing NBS987 without amplifier rotation is 0.710244 ± 0.000014 (2SD, *N*=39).

We note that prior analyses of the AVON2/3 cruise samples from Rose (AVON2/3-66-1) and Malulu (AVON2/3-67-11), reported in **Jackson et al. (2010)**, should be replaced by new analyses of these two samples shown in **Table S1**, for two reasons: 1) the previously published Pb isotopic analyses were made by TIMS without a spike addition to control for in-run mass fractionation and 2) these two samples exhibit significant alteration and acid leaching for the prior analyses may not have been sufficient to have removed alteration phases. We note that the new $^{143}Nd/^{144}Nd$ analysis for AVON2/3-67-11 (0.512982) shows significant disagreement with the prior analysis (0.512796, after correction to the JNdi reference frame use here by applying

the La Jolla to JNdi conversion from **Tanaka et al., 2000**) made at WHOI in the year 2000 and reported by **Jackson et al. (2010)**. In order to evaluate the accuracy of the new $^{143}Nd/^{144}Nd$ measurement, three additional aliquots of this sample were obtained from the WHOI dredge repository, including the original bag of crushed rock chips for this sample from which material was extracted for the 2000 analysis (see AVON2/3-67-11 rep1, rep2, and rep3 in **Table S1**); new batches of chips were prepared by separately crushing each aliquot, and the different aliquots of chips were leached and underwent wet chemistry and mass spectrometry during a separate session than the original analyses. The three replicate $^{143}Nd/^{144}Nd$ analyses (0.512982, 0.512980, and 0.512981) show excellent agreement with the new $^{143}Nd/^{144}Nd$ result, confirming its accuracy. We note that the new analyses of Sr and Pb isotopes for this sample are similar to the published data for this sample reported in **Jackson et al. (2010)**.

Using the Pb fractions purified at UCSB, Pb isotopic analyses were carried out at the Woods Hole Oceanographic Institution using the Thermo Neptune MC-ICP-MS housed there (**Hart and Blusztajn, 2006**). Fractionation correction was made by Tl-addition assuming an exponential fractionation law (**White et al., 2001**). Samples and an aliquot of AGV-2 (processed through all steps of column chemistry and mass spectrometry with the samples) were corrected for the offset between preferred (i.e., values from **Eisele et al., 2003**) and measured ratios of NBS981.

For a different subset of samples (specified in **Table S2**), Pb fractions purified at UCSB were carried out at the University of South Carolina on Thermo Neptune MC-ICP-MS housed there. The samples, together with an aliquot of BCR-2 (processed through all steps of column chemistry and mass spectrometry with the samples) were corrected for the offset between preferred (i.e., values from **Eisele et al., 2003**) and measured ratios of NBS981.

Sr, Nd, Hf and Pb isotopic and major and trace element concentrations on clinopyroxenes from samples EX1702-D12-5 and EX1702-D7-5 at U. South Carolina.

Following leaching, visually fresh clinopyroxenes were picked under a binocular microscope. The clinopyroxene samples were then processed at the Center for Elemental Mass Spectrometry, University of South Carolina. Approximately 150-200 mg of sample was first leached (using the same protocol described above) and dissolved in Teflon distilled $HF:HNO_3$ (3:1) mixture on a hot plate for ~ 3 days, with frequent sonication. After drydown the samples were picked in 6N HCl with added boric acid in 10N HCl to complex fluorides, which increases yields in Hf chemistry (**Frisby et al., 2016**). Afterwards the samples were converted to nitrates. A small aliquot (~5%) was taken for Sr and Nd isotopes and the remainder was dried down with HBr for Pb and then Hf chemistry. A precisely determined aliquot of the dissolved clinopyroxene samples was pipetted from the solution and gravimetrically diluted for trace element analyses prior to the splitting of Sr-Nd and Pb-Hf fractions. Trace elements were then analyzed by ICP-MS with an aliquot of BHVO-1 on the Element2 following established methods for the lab (e.g. **Frisby et al, 2016**).

For the chemical separations, Sr was separated first on an Eichrom Sr-spec resin and the washes containing the rest of the elements were processed through an Eichrom TRU spec resin to concentrate the LREEs, and then on an Eichrom Ln-Resin to isolate Nd (**Frisby et al, 2016**). The Pb was separated on anion resin in HBr and HCl media, and the washes from that were processed for Hf following the method of **Munker et al. (2001)**. An unleached BCR-2 powder was dissolved and processed through all steps of chemistry and mass spectrometry with sample unknowns. Total procedural blanks during the analytical session were 10 pg for Pb, 180 pg for

Sr, <10 pg for Nd, and 40 pg for Hf.

The isotopic compositions of Sr, Nd, Pb, and Hf were measured on the Thermo Neptune housed at the University of South Carolina following methods provided in **Beguelin et al., (2017)**. All samples were corrected for mass bias using the exponential law: Pb was corrected using the Tl addition method (**White et al., 2001**), $^{87}Sr/^{86}Sr$ was corrected using $^{86}Sr/^{88}Sr$ of 0.1194, $^{143}Nd/^{144}Nd$ was corrected using $^{146}Nd/^{144}Nd$ of 0.7219, and $^{176}Hf/^{177}Hf$ was corrected using $^{179}Hf/^{177}Hf$ of 0.7325. All isotopic data on samples were corrected for the offset between measured and preferred standards using the following preferred values: SRM981 values from **Eisele et al. (2003)** ($^{206}Pb/^{204}Pb$ = 16.9409, $^{207}Pb/^{204}Pb$ = 15.4976, and $^{208}Pb/^{204}Pb$ = 36.7262); NBS987 $^{87}Sr/^{86}Sr$ value of 0.710240; JMC-475 $^{176}Hf/^{177}Hf$ value of 0.282160; JNdi $^{143}Nd/^{144}Nd$ value of 0.512099 (**Garçon et al., 2018**).

During the course of these measurements, reproducibility of $^{87}Sr/^{86}Sr$ on NBS987 was 22 ppm, of $^{143}Nd/^{144}Nd$ on JNdi-1 was 20 ppm, of $^{176}Hf/^{177}Hf$ on JMC-475 was 28 ppm, and Pb isotopic compositions on NBS981 were 62ppm on $^{206}Pb/^{204}Pb$, 68 ppm for $^{207}Pb/^{204}Pb$, and 80 ppm for $^{208}Pb/^{204}Pb$ (all 2SE). An unleached BCR-2 powder was run together with the clinopyroxenes through all steps of column chemistry and mass spectrometry, and data are shown in **Table S1**.

Whole rock major and trace element analyses at Washington State University.

For samples EX1702-D7-2, EX1702-D3-2, and EX1702-D11-1, 10 to 20 g blocks of rock were cut with the rock saw, and care was taken to avoid visibly altered portions of rock. The blocks were cleaned with silicon carbide sand paper, and sonicated in MilliQ H_2O. Samples were crushed and then powdered in an agate shatterbox (with cleaning with silica between barrels) at the Geoanalytical lab at the Washington State University (WSU). Major and trace element concentrations were obtained at WSU by X-ray fluorescence (XRF) and ICP-MS. XRF and ICP-MS methods, and evaluation of accuracy using international standards, are reported elsewhere (**Knaack et al., 1994; Johnson et al., 1999**), but summarized briefly here. The precision (1σ) for major elements in basalts by XRF is 0.11–0.33% (1σ) of the amount present for SiO_2, Al_2O_3, TiO_2, P_2O_5) and 0.38–0.71% for other elements. Trace element precision of basalts by ICP-MS is 0.77–3.2% (1σ) for trace elements except for U (9.3%) and Th (9.5%). An aliquot of the USGS reference material BCR-2 was analyzed as an unknown together with the basaltic unknowns, and the data are reported in **Table S2**. The new analysis of BCR-2 reported here is compared major and trace element compositions for this reference material reported in **Jochum et al. (2016)**. Whole rock major and trace element analyses of the AVON2/3-67-1, AVON2/3-66-1, AVON2/3-65-18 and ALIA-DR129-05 were made following the same methods and data are reported in **Jackson et al. (2010)**.

In situ major element analyses on glass by electron microprobe at UC Santa Barbara.

Glass was available for EX1702-D3-2. Sample chips were analyzed by electron microprobe at UC Santa Barbara using primary standards and following analytical conditions outlined in **Jackson et al. (2015)**. The MORB basaltic secondary standard 519-4-1 was analyzed repeatedly throughout the analytical session. Major element compositions for sample unknown glass and the secondary standard (and previously published data on this secondary standard from **Melson et al., 2002**) are reported in **Table S2**.

In situ trace element analyses by LA-ICP-MS at Clermont-Ferrand.

Trace element analyzes on the EX1702-D3-2 glass sample were made using a laser ablation ICP-MS system housed at Laboratoire Magmas et Volcans at Clermont-Ferrand. Analytical methods are outlined in **Oulton et al. (2016)** and **Reinhart et al. (2018)**. Analyses were made using a Thermo Scientific Element XR ICP-MS coupled to a Resonetics M-50E 193 nm ArF excimer laser. ^{43}Ca was used as an internal standard. All surfaces were preablated (for 1s at 10Hz) prior to analysis. Analyses of samples and standards used a 47 μm laser spot, and the laser was fired with a 4 Hz repetition rate. Analyses were conducted over 80 second ablation periods, with 20 seconds of blank analysis (with the laser off) before samples analysis and (following a washout period) 20 seconds of blank analysis (again, with the laser off) after the analysis. Analyses were made in low resolution mode using triple mode with a 20% mass window and a 20 ms integration window. Acceleration voltage was scanned between magnet scans to ensure peak positions were maintained. Calibration curves were generated using NIST612 (**Gagnon et al., 2008**) and BCR-2 (**Jochum et al., 2006)** glass. Replicate analyses of a MORB glass, 519-4-1, were made throughout the analytical session to monitor precision and accuracy of analyses. The reproducibility of the trace element analyses was better than 10% (2RSD, N=8) for all elements except for Cs (44%). Measured concentrations are compared with previously published analyses from **Gale et al. (2013)** in **Table S2**.

Figure Captions

Figure S1. Isotopic data for volcanoes in this study plotted with existing data for Macdonald and Arago volcanoes. The Rose atoll, Malulu seamount, and Dino seamount are all geochemically linked to the Macdonald hotspot, consistently grouping with Macdonald-type volcanoes. The Moki seamount falls into the region where the Macdonald and Arago isotope spaces overlap in all plots except for the plot of ^{176}Hf/^{177}Hf versus ^{143}Nd/^{144}Nd where it clearly links to Macdonald. A hotspot origin for Papatua cannot be determined as it consistently plots in the region of overlap between Macdonald and Arago isotope spaces. The Moki and Malulu isotopic data produced for this study are from clinopyroxene phenocrysts, as seawater alteration prevented the analysis of whole rock samples. New data also include pillow rim glass analyses from Rose atoll, whole rock data from Dino seamount, and new whole rock data on Rose and Malulu lavas. Whole rock data for the Rose atoll and the Malulu and Papatua seamounts was published by Jackson et al., 2010. All data not produced by this study was previously published and downloaded from Georoc (http://georoc.mpch681mainz.gwdg.de/georoc). Figure modified after Jackson et al. (2020).

Figure S2. Age-distance relationship for Arago and Macdonald volcanoes, with projected ages for interloper volcanoes Moki, Malulu, Dino, Papatua, and the Rose atoll for both Macdonald and Arago plume origin. Hawaiian hotspot data are shown for reference. This figure uses the great circle distances between current hotspot locations and a related volcano along the Wessel and Kroenke (2008) reconstructed trends. The volcanoes in this study plot in between the CAVL Macdonald volcanoes and the Macdonald hotspot-related Tokelau islands, suggesting that they bridge a geographic gap in Macdonald-type isotope geochemistry. Ages have been estimated for the five interloper volcanoes, based on the location of each volcano on the along-track distance trends, for both a Macdonald and Arago hotspot origin. Assuming Macdonald origin for all seamounts and the Rose atoll, Moki is ~51 Ma, Papatua is ~46 Ma, Malulu is ~44 Ma, Rose atoll is ~43 Ma, and Dino is ~39 Ma. Assuming Arago

origin, Moki is ~27 Ma, Papatua is ~25 Ma, Malulu is ~23 Ma, Rose atoll is ~22 Ma, and Dino is ~21 Ma. Age data used in this plot are provided in Jackson et al. (2020). Figure modified after Jackson et al. (2020).

Figure S3. Total alkali versus SiO_2 diagram for whole rock lavas analyzed in this study. Whole rock data from other Cook-Austral volcanoes are shown for reference. The dashed line represents the boundary between the alkali (above the line) and tholeiitic (below the line) fields. The samples analyzed here plot broadly in the region defined by other volcanoes from the Cook-Austral volcanic lineament. Major elements are shown as normalized to 100% totals on a volatile-free basis. Major element data for the Malulu hyaloclastite (EX1702-12-5) are not shown, as only clinopyroxenes were analyzed.

Figure S4. Trace element spider diagrams for whole rock and clinopyroxene samples from study volcanoes. Trace element concentrations are normalized to pyrolite from McDonough and Sun (1995). Whole rocks are shown in the top panel, and clinopyroxenes in the lower panel.

References Cited

Beguelin, P., M. Bizimis, C. Beier, and S.Turner, 2017, Rift–plume interaction reveals multiple generations of recycled oceanic crust in Azores lavas. *Geochimica et Cosmochimica Acta,* v. 218, p. 132–152.

Eisele, J., Abouchami, W., Galer, S.J.G., and Hofmann, A.W., 2003, The 320 kyr Pb isotope evolution of Mauna Kea lavas recorded in the HSDP-2 drill core. *Geochemistry, Geophysics, Geosystems*, v. 4, 8710, doi:10.1029/2002GC000339.

Frisby, C., Bizimis, M. and Mallick, S., 2016, Hf–Nd isotope decoupling in bulk abyssal peridotites due to serpentinization. *Chemical Geology*, v. 440, p. 60-72.

Gagnon, J.E., Fryer, B.J., Samson, I.M., Williams-Jones, A.E., 2008, Quantitative analysis of silicate certified reference materials by LA-ICPMS with and without an internal standard. *Journal of Analytic Atomic Spectrometry*, v. 23, p. 1529–1537.

Gale, A., M. Laubier, S. Escrig, and C. H. Langmuir, 2013, Constraints on melting processes and plume-ridge interaction from comprehensive study of the FAMOUS and North Famous segments, Mid-Atlantic Ridge. *Earth and Planetary Science Letters*, v. 365, p. 209–220, doi:10.1016/801j.epsl.2013.01.022.

Garçon, M., Boyet, M., Carlson, R.W., Horan, M.F., Auclair, D., and Mock, T.D., 2018, Factors influencing the precision and accuracy of Nd isotope measurements by thermal ionization mass spectrometry. *Chemical Geology*, v. 476 p. 493–514.

Hart, S.R., and Blusztajn, J., 2006, Age and geochemistry of the mafic sills, ODP site 1276, Newfoundland margin. *Chemical Geology*, v. 235, p. 222–237.

Jackson, M.G., Hart, S.R., Konter, J.G., Koppers, A.A.P., Staudigel, H., Kurz, M.D., Blusztajn,

J., and Sinton, J.M., 2010, The Samoan hotspot track on a “hotspot highway”: Implications for mantle plumes and a deep Samoan mantle source. *Geochemistry, Geophysics, Geosystems*, v. 11, Q12009, doi:10.1029/2010GC003232.

Jackson, M.G., Koga, K.T., Price, A., Konter, J.G., Koppers, A.A.P., Finlayson, V.A., Konrad, K., Hauri, E.H., Kylander-Clark, A., Kelley, K.A., and Kendrick, M.A., 2015, Deeply-dredged submarine HIMU glasses from the Tuvalu Islands, Polynesia: Implications for volatile budgets of recycled oceanic crust. *Geochemistry, Geophysics, Geosystems*, v. 16, p. 3210-3234, DOI: 10.1002/2015GC005966.

Jackson, M.G., Halldórsson, S.A., Price, A., Kurz, M.D., Konter, J.G., Koppers, A.A.P., Day, J.M.D., 2020, Contrasting old and young volcanism from Aitutaki, Cook Islands: Implications for the origins of the Cook-Austral volcanic chain. Journal of Petrology, egaa037, https://doi.org/10.1093/petrology/egaa037.

Jochum, K., Stoll, B., Herwig, K., Willbold, M., Hofmann, A., Amini, M., Aarburg, S., Abouchami, W., Hellebrand, E., Mocek, B., Raczek, I., Stracke, A., Alard, O., Bouman, C., Becker, S., Dücking, M., Brätz, H., Klemd, R., Bruin, D., Canil, D., Cornell, D., Hoog, C.-J., Dalpe, C., Danyushevsky, L., Eisenhauer, A., Gao, Y., Snow, J., Groschopf, N., Günther, D., Latkoczy, C., Guillong, M., Hauri, E., Höfer, H., Lahaye, Y., Horz, K., Jacob, D., Kasemann, S., Kent, A., Ludwig, T., Zack, T., Mason, P., Meixner, A., Rosner, M., Misawa, K., Nash, B., Pfänder, J., Premo, W., Sun, W., Tiepolo, M., Vannucci, R., Vennemann, T., Wayne, D., and Woodhead, J., 2006, MPIDING reference glasses for in situ microanalysis: new reference values for element concentrations and isotope ratios. *Geochemistry, Geophysics, Geosystems*, v. 7, Q02008.

Jochum, K., Weis, U., Schwager, B., Stoll, B., Wilson, S.A., Haug, G.H., Andreae, M.O., Enzweiler, J., 2016, Reference values following ISO guidelines for frequently requested rock reference materials. *Geostandards and Geoanalytical Research*, v. 40, p. 333-350.

Johnson, D.M., Hooper, P.R., and Conrey, R.M., 1999, XRF analysis of rocks and minerals for major and trace elements in a single low dilution Li-tetraborate fused bead. *Advances in X-Ray Analysis*, v. 41, p. 843–867.

Knaack, C.M., Cornelius, S.B., and Hooper, P.R., 1994, Trace element Analysis of rocks and minerals by ICP-MS. Open File Report, GeoAnalytical Lab. Washington State University, p. 10.

McDonough, W.F., Sun, S.S., 1995, The composition of the Earth. *Chemical Geology*, v. 120, p. 223-253.

Melson, W.G., O'Hearn, T., and Jarosewich, E., 2002, A data brief on the Smithsonian Abyssal Volcanic Glass Data File. *Geochemistry, Geophysics, Geosystems*, v. 3, p. 1-11, doi:10.1029/2001GC000249.

Munker, C., Weyer, S., Scherer, E. and Mezger, K., 2001, Separation of high field strength

elements (Nb, Ta, Zr, Hf) and Lu from rock samples for MC-ICPMS measurements. *Geochemistry, Geophysics, Geosystems*, v. 2, p. 1064, doi:10/1029:2001GC000183.

Oulton, J., Humayun, M., Fedkin, A., and Grossman, L., 2016, Chemical evidence for differentiation, evaporation and recondensation from silicate clasts in Gujba. *Geochimica et Cosmochimica Acta*, v. 177, p. 254–274.

Price, A.A., Jackson, M.G., Blichert-Toft, J., Hall, P.S., Sinton, J.M., Kurz, M.D., and Blusztajn, J., 2014, Evidence for a broadly distributed Samoan-plume signature in the northern Lau and North Fiji Basins. *Geochemistry, Geophysics, Geosystems*, v. 15, p. 986-1008, doi: 10.1002/2013GC005061.

Price, A.A., Jackson, M.G., Blichert-Toft, J., Blusztajn, J., Conatser, C.S., Konter, J.G., Koppers, A.A.P., and Kurz, M.D., 2016, Geochemical evidence in the Northeast Lau Basin for subduction of the Cook-Austral volcanic chain in the Tonga Trench. *Geochemistry, Geophysics, Geosystems*, v. 17, p. 1694-1724, doi:10.1002/2015GC006237.

Reinhard, A.A., Jackson, M.G., Koornneef, J.M., Rose-Koga, E.F., Blusztajn, J., Konter, J.G., Koga, K.T., Wallace, P.J., Harvey, J., 2018, Sr and Nd isotopic compositions of individual olivine-hosted melt inclusions from Hawai'I and Samoa: Implications for the origin of isotopic heterogeneity in melt inclusions from OIB lavas. *Chemical Geology*, v. 495, p. 36-49.

Tanaka, T., Togashi, S., Kamioka, H., Amakawa, H., Kagami, H., Hamamoto, T., Yuhara, M., Orihashi, Y., Yoneda, S., Shimizu, H., Kunimaru, T., Takahashi, K., Yanagi, T., Nakano, T., Fujimaki, H., Shinjo, R., Asahara, Y., Tanimizu, M., and Dragusanu, C., 2000, JNdi-1: A neodymium isotopic reference in consistency with LaJolla neodymium. *Chemical Geology*, v. 168, p. 279–281.

Weis, D., Kieffer, B., Maerschalk, C., Barling, J., de Jong, J.. Williams, G.A., Hanano, D., Pretorius, W., Mattielli, N., Scoates, J.A., Goolaerts, A., Friedman, R.M., Mahoney, B.J., 2006, High-precision isotopic characterization of USGS reference materials by TIMS and MC-ICP-MS. *Geochemistry, Geophysics, Geosystems*, v. 7, Q08006.

Weis, D., Kieffer, B., Hanano, D., Silva, I.N., Barling, J., Pretorius, W., Maerschalk, C., Matielli, N., 2007, Hf isotope compositions of U.S. Geological Survey reference materials. *Geochemistry, Geophysics, Geosystems*, v. 8, Q06006.

Wessel, P., and Kroenke, L.W., 2008, Pacific absolute plate motion since 145Ma: an assessment of the fixed hot spot hypothesis. *Journal of Geophysical Research*, v.113, B06101. https://doi.org/10.1029/2007JB005499.

White, W.M., Albarede, F. and Telouk, P., 2000, High-precision analysis of Pb isotope ratios by multi-collector ICP-MS. *Chemical Geology*, v. 167, p. 257-270.

Table S1. Radiogenic isotopic compositions for whole rocks, glass, and clinopyroxene separates from non-Samoan "interloper" seamounts in the Samoan region.[1]

Sample ID	Volcano name	Material analyzed	Latitude	Longitude	$^{87}Sr/^{86}Sr$	2SE	$^{143}Nd/^{144}Nd$	2SE	$^{176}Hf/^{177}Hf$	2SE	$^{206}Pb/^{204}Pb$	2SE	$^{207}Pb/^{204}Pb$	2SE	$^{208}Pb/^{204}Pb$	2SE
EX1702-D7-2 [2]	Moki smt.	cpx	-11.1682	-169.8922	0.703037	0.000005	0.512908	0.000005	0.282922	0.000003	20.2209	0.0016	15.6205	0.0012	40.0478	0.0031
EX1702-D7-2 rep [3]	Moki smt.	cpx	-11.1682	-169.8922	0.703034	0.000005	0.512911	0.000004								
EX1702-D11-1 [3]	Smt D (Dino)	whole rock	-15.7331	-167.2646	0.702872	0.000009	0.512989	0.000005			19.6917	0.0029	15.6201	0.0025	39.2270	0.0059
EX1702-D11-1 rep [4]	Smt D (Dino)	whole rock	-15.7331	-167.2646	0.702795	0.000003	0.512985	0.000004			19.7050	0.0078	15.6162	0.0069	39.3336	0.0198
EX1702-D3-2 [4]	Rose atoll	glass	-14.5377	-168.0799	0.704014	0.000003	0.512817	0.000003			19.2401	0.0005	15.6203	0.0005	39.0252	0.0017
AVON2/3-D66-1 [3]	Rose atoll	whole rock	-14.6433	-168.1956	0.704085	0.000006	0.512798	0.000003			19.1025	0.0058	15.5980	0.0047	38.9144	0.0107
AVON2/3-D66-1 [5]	Rose atoll	whole rock	-14.6433	-168.1956	*0.704137*		*0.512796*				*19.14*		*15.62*		*38.98*	
AVON2/3-D65-18 [5]	Rose atoll	whole rock	-14.4890	-168.2609	*0.703923*		*0.512846*				*19.32*		*15.61*		*39.1615*	
EX1702-D12-5 [2]	Malulu smt	cpx	-14.4689	-168.6389	0.703121	0.000005	0.512979	0.000003	0.283051	0.000004	19.7237	0.0007	15.5812	0.0007	39.4479	0.0018
EX1702-D12-5 rep [4]	Malulu smt	cpx	-14.4689	-168.6389	0.703101	0.000003	0.512982	0.000002			19.7483	0.0059	15.5877	0.0056	39.4271	0.0162
AVON2/3-D67-11 [3]	Malulu smt	whole rock	-14.4988	-168.6631	0.703096	0.000006	0.512982	0.000003								
AVON2/3-D67-11 rep1 [3]	Malulu smt	whole rock	-14.4988	-168.6631	0.703100	0.000007	0.512982	0.000003			20.9563	0.0024	15.6535	0.0017	40.9142	0.0048
AVON2/3-D67-11 rep2 [3]	Malulu smt	whole rock	-14.4988	-168.6631	0.703108	0.000006	0.512980	0.000003								
AVON2/3-D67-11 rep3 [3]	Malulu smt	whole rock	-14.4988	-168.6631	0.703102	0.000007	0.512981	0.000003								
AVON2/3-D67-11 [5]	Malulu smt	whole rock	-14.4988	-168.6631	*0.703108*		*0.512765* [7]				*20.96*		*15.66*		*40.71*	
ALIA-DR129-05 [6]	Papatua smt	whole rock	-14.9705	-170.5900	*0.703009*		*0.512976*				*20.0614*		*15.6561*		*39.6569*	
BCR-2 [2]		powder			0.705010	0.000004	0.512623	0.000010	0.282873	0.000003	18.7561	0.0026	15.6210	0.0032	38.7311	0.0035
BCR-2 [3]		powder			0.705007	0.000006	0.512621	0.000002								
BCR-2 [3]		powder			0.705003	0.000006	0.512620	0.000002			18.7543	0.0004	15.6188	0.0004	38.7162	0.0013
BCR-2 [3]		powder			0.705006	0.000006	0.512625	0.000003			18.7415	0.0004	15.6093	0.0004	38.6795	0.0013
BCR-2 published (Weis et al. 2006, 2007) [1]		powder			0.705005	0.000010	0.512621	0.000012	0.282870	0.000008	18.7533	0.0195	15.6262	0.0040	38.7282	0.0405
AGV-2 [4]		powder			0.703981	0.000004	0.512776	0.000002			18.8704	0.0010	15.6215	0.0009	38.5527	0.0025
AGV-2 published (Weis et al. 2006, 2007) [1]		powder			0.703973	0.000009	0.512775	0.000010			18.8692	0.0063	15.6186	0.0071	38.5488	0.0135

1. All data in the table are reported relative to the following international standard values: Nd isotopes are corrected to JNdi value of 0.512099 (**Garcon et al., 2018**), Sr isotopic data to an NBS 987 value of 0.710240, Pb isotopic compositions are corrected to the NIST 981 values of **Eisele et al. (2003)** (16.9409, 15.4976, 36.7262), and Hf isotopic data are corrected to the JMC-475 of 0.282160. For the data from **Weis et al (2006, 2007)**, Nd isotopic compositions are renormalized to a JNdi equivalent value of 0.512099 using **Tanaka et al.'s (2000)** La Jolla to JNdi-1 conversion, and their Pb isotopic data are renormalized to the NBS981 values from **Eisele et al. (2003)**, and only teflon data are shown for the Hf isotopic dataset. Italicized data are previously published from **Jackson et al (2010)**, and represent Sr, Nd, and unspiked Pb run by TIMS at WHOI (and are renormalized to the international standard values provided above). For the **Weis et al (2006, 2007 data)**, errors are reported as 2SD of multiple analyses (all other errors in the table are 2SE), except for the BCR analysis at University of South Carolina (which is the 2SD of 5 analyses of the same BCR-2).
2. All leaching, wet chemistry (sample dissolutions and chemical separations) and mass spectrometry (all using MC-ICP-MS) for Sr, Nd, Pb and Hf isotopes completed at U. South Carolina.
3. Leaching and wet chemistry (sample dissolutions and chemical separations) for Sr, Nd, and Pb completed at UCSB. Sr and Nd mass spectrometry completed on UCSB TIMS, and Pb mass spectrometry (if any) completed on U. South Carolina MC-ICP-MS.
4. Leaching and wet chemistry (sample dissolutions and chemical separations) for Sr, Nd, and Pb completed at UCSB. Sr and Nd mass spectrometry completed on UCSB TIMS, and Pb mass spectrometry (if any) completed on WHOI MC-ICP-MS.
5. Leaching and wet chemistry (sample dissolutions and chemical separations) and mass spectrometry for Sr, Nd, and Pb completed on WHOI TIMS (data published in **Jackson et al., 2010)**.
6. Leaching and wet chemistry (sample dissolutions and chemical separations) and mass spectrometry for Sr, Nd, and Pb completed on WHOI MC-ICP-MS (data published in **Jackson et al., 2010)**.
7. This result is superceded by new analyses of this sample made at UCSB (also presented in this table).

Table S2. Major and trace element concentrations lavas published in this study together with prior analyses of related seamounts.

Seamount or atoll	Moki smt. [1]	Moki smt. [2]	Papatua smt. [3]	Malulu smt. [3]	Malulu smt. [2]	Smt. D (Dino) [1]	Rose atoll [3]	Rose atoll [3]	Rose atoll [1]	Rose atoll [4]	Ref material [1]	Ref material [1]	Ref material [2]	Ref material [2]	Ref material [4]	Ref material [4]
Sample ID	EX1702-D7-2	EX1702-D7-2	ALIA-DR129-05	AVON2/3-67-11	EX1702-12-5	EX1702-D11-1	AVON2/3-65-18	AVON2/3-66-1	EX1702-D3-2	EX1702-D3-2	BCR-2	BCR-2	BHVO-1	BHVO-1	ALV-519-4-1	ALV-519-4-1
Sample Info	whole rock	cpx	whole rock	whole rock	cpx	whole rock	whole rock	whole rock	whole rock	glass	(this study)	(publ)	(this study)	(publ)	(this study)	(publ)
XRF or ICP-MS Solution Majors																
SiO_2	36.30		*38.65*	*41.77*		45.00	*45.97*	*46.18*	46.43	51.57	54.30	54.93		50.17	48.98	48.94
TiO_2	4.736		*3.43*	*3.20*		1.820	*3.11*	*1.90*	2.440	2.43	2.29	2.30		2.76	0.73	0.77
Al_2O_3	12.34		*15.67*	*11.63*		15.52	*13.26*	*8.89*	13.85	14.61	13.54	13.71		13.80	16.44	16.53
FeO*	11.37		*10.84*	*13.56*		8.88	*11.45*	*11.53*	11.83	9.54	12.47	12.61		11.17	8.91	9.03
MnO	0.125		*0.18*	*0.22*		0.061	*0.17*	*0.18*	0.154	0.14	0.20	0.20		0.17	0.17	
MgO	6.59		*3.33*	*7.09*		2.43	*8.46*	*19.18*	6.43	6.13	3.60	3.66		7.27	9.71	9.41
CaO	15.15		*10.66*	*15.64*		12.60	*11.22*	*9.17*	11.30	10.16	7.15	7.24		11.52	12.48	12.58
Na_2O	1.17		*3.14*	*1.95*		3.01	*2.03*	*1.47*	2.89	3.05	3.18	3.17		2.33	2.10	2.07
K_2O	0.83		*1.96*	*1.11*		2.42	*1.50*	*0.58*	0.54	0.91	1.80	1.80		0.53	0.08	0.1
P_2O_5	2.586		*3.26*	*1.50*		0.594	*0.27*	*0.24*	0.893	0.39	0.35	0.37		0.28	0.07	0.09
Total (majors only)	91.18		*91.13*	*97.67*		92.43	*97.44*	*99.32*	96.77	98.92	98.86				99.66	99.52
LOI	8.11		*8.87*	*2.33*		7.27	*2.56*	*0.68*	2.78							
Sum of Majors and LOI	99.29		100.00	100.00		99.69	100.00	100.00	99.55							
XRF or ICP-MS Solution or Laser Traces																
Ni	86		*44*	*120*		28	*148*	*692*	144	84	12	13			189	178
Cr	456	1922	*3*	*608*	1430	34	*437*	*1116*	726	160	11	16	292	288	413	526
V	366	208	*224*	*319*	139	196	*278*	*182*	240	230	410	418	321	314	244	210
Ga	18	7.5	*17*	*16*	11.1	17	*17*	*18*	22	23	22	22	21	21	14	
Cu	92	1.5	*54*	*148*	1.9	117	*78*	*54*	68	57	18	20	130	137	108	98
Zn	218	15	*174*	*144*	25	99	*151*	*116*	158	144	130	130	106	105	83	
Sc	36					43			26		33	1				
Ba	220					90			155		687	684				
Nb	82					13			24		13	12				
Rb	18					32			9		47	46				
Sr	279					266			462		338	337				
Zr	266					128			187		178	187				
Y	59					32			31		36	1				
La	75					13			23		25	25				
Ce	113					26			50		55	53				
Nd	55					19			32		29	28				
ICP-MS Solution or Laser Traces																
Li		0.47			1.54					8.21			4.76	4.68	4.22	4.20
Mo		0.03			0.11								1.07	1.06		
Sn		0.06			0.20								1.79	2.09		
W		bdl			0.02								0.20	0.21		
Co		24.8			21.6					37.3			43.6	44.9	51.2	48.7
Cs	0.52	bdl	*1.54*	*0.96*	0.00	0.76	*0.38*	*0.31*	0.20	0.59	1.14	1.16	0.09	0.10	0.02	0.02
Rb	17.4	bdl	*37.2*	*28.7*	0.15	30.1	*21.2*	*12.4*	7.18	25.5	46.5	46.0	8.24	9.52	2.13	2.01
Ba	219	0.72	*292*	*257.4*	2.93	90.7	*65.9*	*103.0*	151	202	683	684	128	134	24.4	24.3
Th	6.24	0.05	*5.74*	*6.40*	0.34	1.14	*3.58*	*1.82*	3.06	2.88	6.23	5.83	1.22	1.23	0.26	0.28
U	2.89	0.01	*1.89*	*1.73*	0.04	0.42	*0.29*	*0.41*	0.79	0.91	1.71	1.68	0.41	0.42	0.09	0.09
Nb	84.7	0.87	*60.7*	*77.8*	3.02	13.1	*33.2*	*19.2*	24.5	27.3	11.6	12.4	20.1	18.5	4.02	4.49
Ta	5.51	0.11	*3.85*	*4.51*	0.43	0.90	*2.35*	*1.32*	1.67	1.66	0.78	0.79	1.17	1.17	0.24	0.27
La	74.3	3.02	*88.1*	*76.1*	9.32	12.9	*26.2*	*15.8*	24.6	22.2	25.7	25.1	15.4	15.4	2.68	2.81
Ce	114	10.2	*101.0*	*145.9*	29.7	26.6	*68.0*	*35.8*	49.6	50.8	53.5	53.1	37.5	38.1	6.75	6.90
Pb	2.39	0.02	*3.59*	*3.40*	0.11	0.89	*2.94*	*1.91*	2.40	2.69	10.4	10.6	2.02	2.04	0.21	0.27
Pr	14.3	1.69	*15.1*	*18.1*	5.02	3.91	*8.16*	*4.50*	6.54	6.19	6.97	6.83	4.93	5.42	0.94	1.02
Nd	56.3	9.16	*61.4*	*77.7*	27.9	17.6	*37.0*	*20.8*	28.9	28.2	29.2	28.3	24.4	24.8	4.86	5.17
Sr	290	55.2	*822*	*1066*	164	272	*145*	*244*	477	458	346	337	390	399	64	71
Zr	280	52.6	*271*	*278*	214	130	*208*	*132*	194	195	184	187	171	175	34.5	39.9
Hf	7.03	2.47	*6.21*	*5.97*	6.95	3.29	*5.71*	*3.46*	5.05	4.49	5.03	4.97	4.26	4.44	0.95	1.11
Sm	10.7	2.51	*12.24*	*17.65*	7.43	4.69	*9.51*	*5.47*	7.29	6.82	6.94	6.55	5.91	6.17	1.62	1.66
Eu	3.38	0.83	*3.93*	*5.68*	2.37	1.76	*3.06*	*1.80*	2.48	2.19	2.13	1.99	2.03	2.05	0.63	0.65
Gd	9.83	2.48	*12.51*	*15.40*	6.79	5.70	*8.69*	*4.99*	7.19	6.36	7.11	6.81	6.20	6.29	2.28	2.58
Tb	1.39	0.38	*1.89*	*2.11*	0.91	0.95	*1.31*	*0.75*	1.09	0.86	1.18	1.08	0.94	0.95	0.42	0.48
Dy	8.05	1.77	*11.72*	*10.79*	4.14	5.96	*6.93*	*4.16*	6.15	5.14	6.99	6.42	4.90	5.27	3.24	3.44
Ho	1.58	0.31	*2.71*	*1.83*	0.65	1.26	*1.20*	*0.74*	1.12	0.90	1.46	1.31	0.94	0.98	0.71	0.79
Y	60.9	8.0	*129.5*	*54.0*	18.0	32.1	*31.6*	*18.5*	31.5	22.8	36.2	36.1	26.2	26.2	18.6	22.3
Er	3.96	0.72	*7.66*	*4.06*	1.37	3.40	*2.81*	*1.71*	2.72	2.31	3.81	3.67	2.44	2.50	2.21	2.33
Tm	0.53	0.09	*1.09*	*0.50*	0.16	0.47	*0.35*	*0.22*	0.37	0.30	0.55	0.53	0.34	0.33	0.33	
Yb	3.22	0.51	*6.89*	*2.71*	0.90	2.88	*1.90*	*1.26*	2.10	1.79	3.34	3.39	1.93	1.99	2.30	2.43
Lu	0.51	0.07	*1.19*	*0.39*	0.12	0.46	*0.28*	*0.18*	0.31	0.24	0.51	0.50	0.27	0.28	0.34	0.39
Sc	35.9	80.8	*14.6*	*28.6*	79.8	44.6	*29.0*	*24.9*	26.4	23.9	33.4	33.5	31.9	31.4	42.6	43.0

1. For whole rock samples EX1702-D7-2, EX1702-D11-1, and EX1702-D3-2, major elements and a subset of trace elements analyzed by XRF, and some of these trace elements and an additional set of trace elements were analyzed by solution ICP-MS. A BCR-2 reference material was analyzed as an unknown together with the samples in this study and previously published data on the BCR-2 are reported in **Jochum et al. (2016)** and shown in this table for reference.
2. Trace elements and a subset of major elements on clinopyroxene separates (EX1702-D7-2 and EX1702-D12-5) were run by solution ICP-MS at the University of South Carolina. Published major and trace element concentrations for this reference materials are from **Jochum et al. (2016)** and are shown in this table for reference; the major element concentrations from **Jochum et al. (2016)** are here normalized to 100% total with all Fe reported as FeO.
3. Italicized data were previously published in **Jackson et al. (2010)**, and include two lavas from Rose atoll, 1 lava from Papatua seamount, and 1 lava from Malulu seamount. LOI's (Loss On Ignition) are estimated for these 4 lavas after **Jackson et al. (2010)**.
4. The major element composition of the EX1702-D3-2 glass is the average of three different spot analyses by electron probe. The major element composition of the ALV-519-4-1 reference glass is the average of 22 different spot analyses analyzed during the same analytical session as EX1702-D3-2, and the data are shown together with published of ALV-519-2 values from **Melson et al (2002)**. The trace element composition of the EX1702-D3-2 glass is the average of four different spot analyses by LA-ICP-MS. The trace element composition of the ALV-519-4-1 reference glass is the average of 8 different spot analyses during the same analytical session as EX1702-D3-2, and the data are shown together with published data on ALV-519-4-1 from **Gale et al. (2013)** and compiled in **Jackson et al. (2015)**.

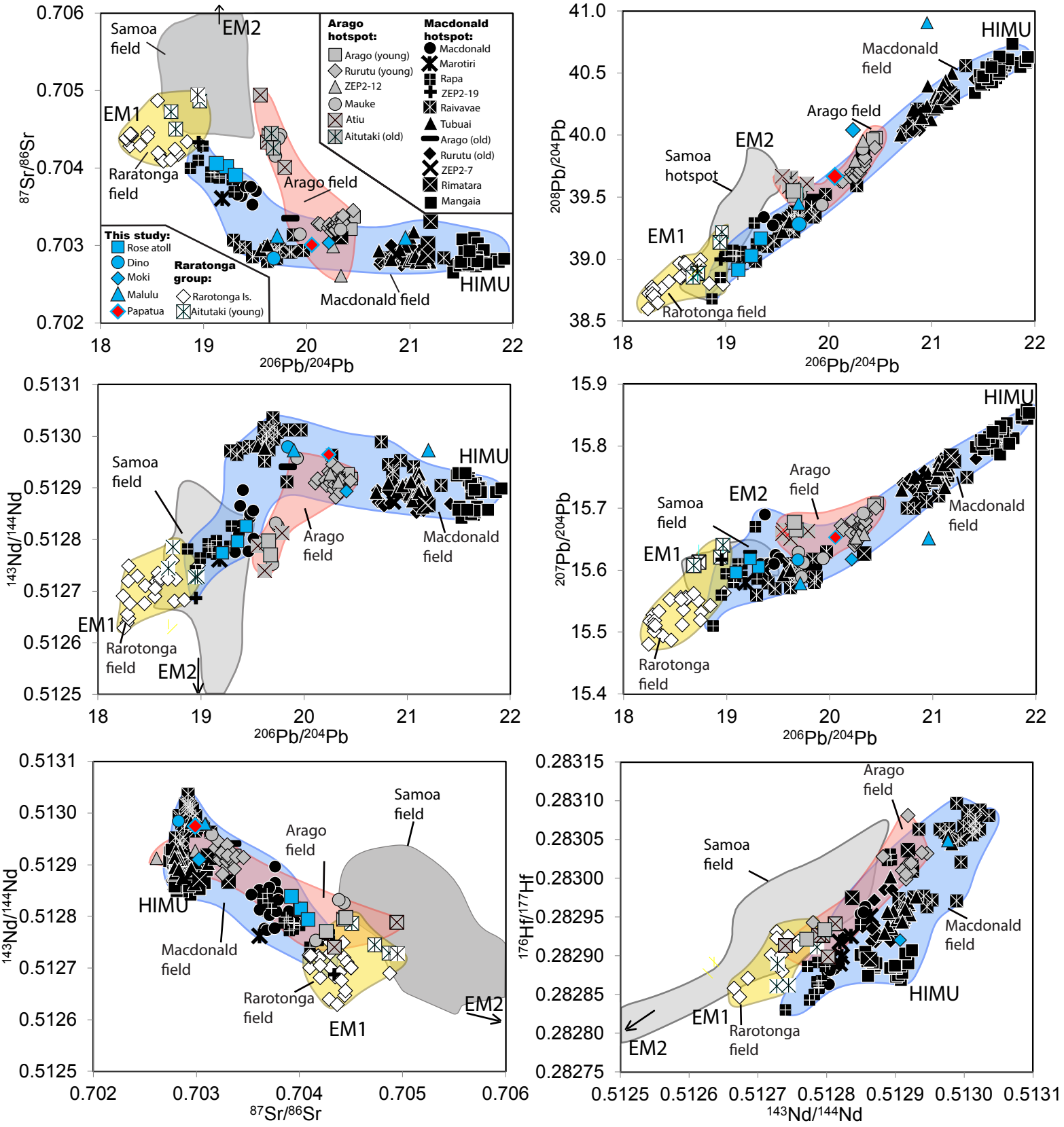
Samoa field
EM2
EM1
Raratonga field
Arago field
Macdonald field
HIMU
Arago hotspot:
Arago (young)
Rurutu (young)
ZEP2-12
Mauke
Atiu
Aitutaki (old)
Macdonald hotspot:
Macdonald
Marotiri
Rapa
ZEP2-19
Raivavae
Tubuai
Arago (old)
Rurutu (old)
ZEP2-7
Rimatara
Mangaia
This study:
Rose atoll
Dino
Moki
Malulu
Papatua
Raratonga group:
Rarotonga Is.
Aitutaki (young)
87Sr/86Sr
206Pb/204Pb
208Pb/204Pb
Samoa hotspot
Rarotonga field
143Nd/144Nd
207Pb/204Pb
176Hf/177Hf

Figure S1

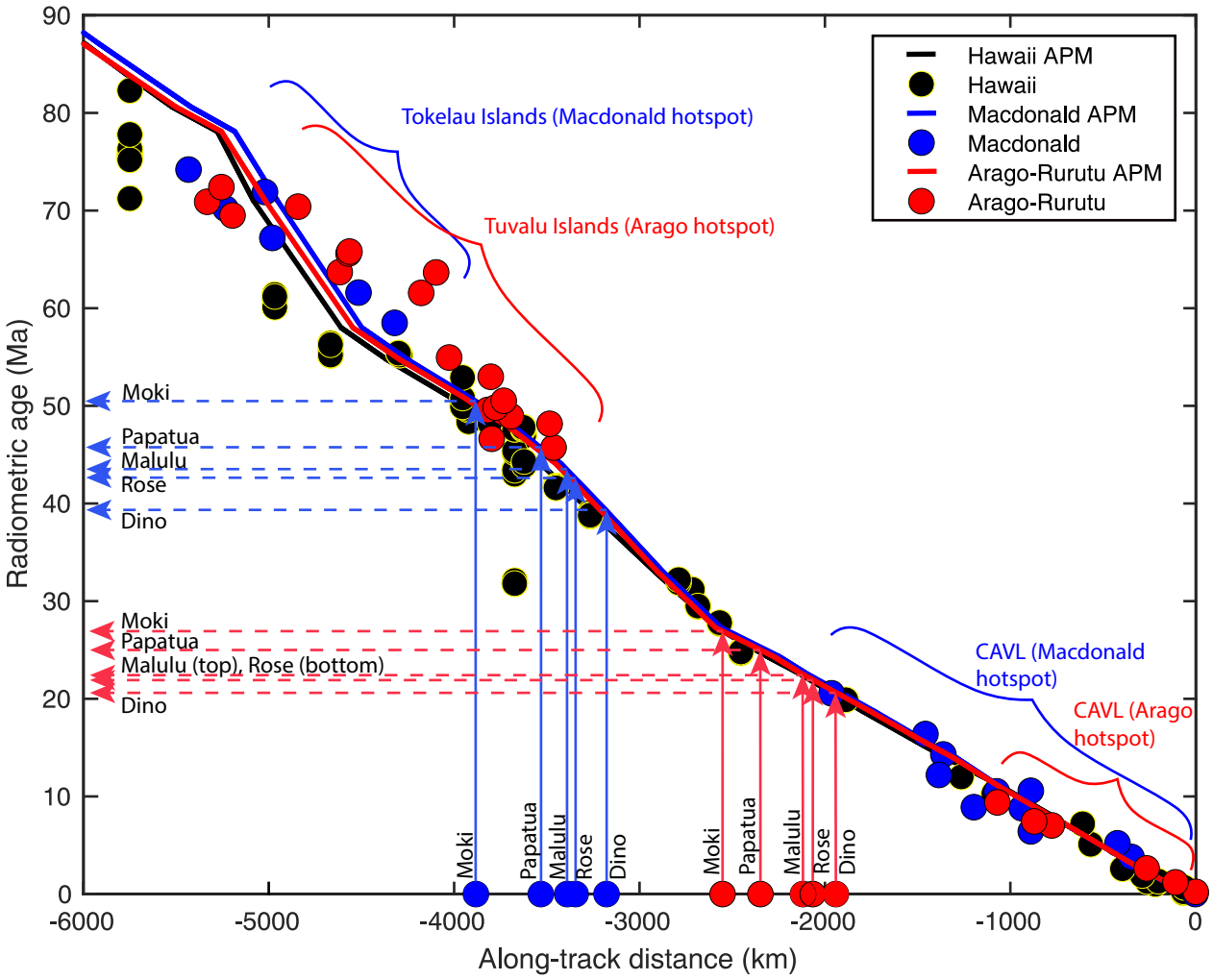
Hawaii APM
Hawaii
Macdonald APM
Macdonald
Arago-Rurutu APM
Arago-Rurutu
Tokelau Islands (Macdonald hotspot)
Tuvalu Islands (Arago hotspot)
CAVL (Macdonald hotspot)
CAVL (Arago hotspot)
Moki
Papatua
Malulu
Rose
Dino
Moki
Papatua
Malulu (top), Rose (bottom)
Dino
Moki
Papatua
Malulu
Rose
Dino
Moki
Papatua
Malulu
Rose
Dino
Radiometric age (Ma)
Along-track distance (km)
0
10
20
30
40
50
60
70
80
90
-6000
-5000
-4000
-3000
-2000
-1000
0

Figure S2

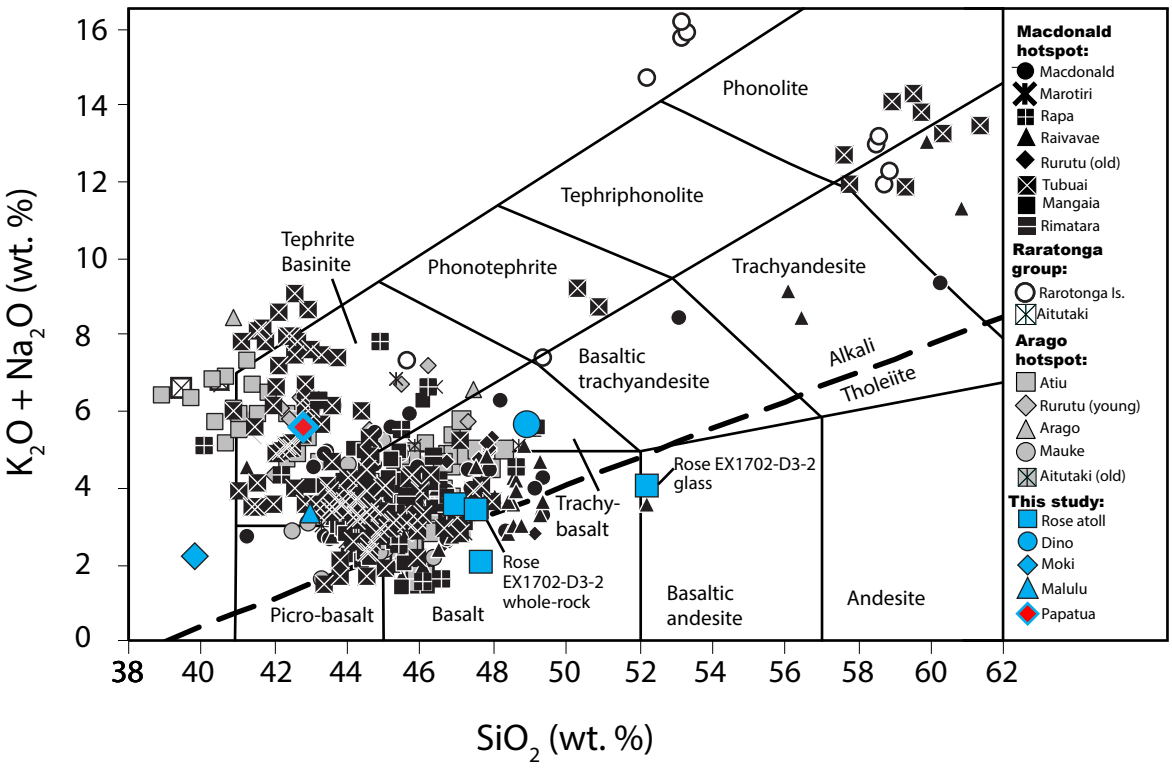
Phonolite
Tephriphonolite
Tephrite
Basinite
Phonotephrite
Trachyandesite
Basaltic
trachyandesite
Alkali
Tholeiite
Rose EX1702-D3-2
glass
Trachy-
basalt
Rose
EX1702-D3-2
whole-rock
Picro-basalt
Basalt
Basaltic
andesite
Andesite
$K_2O + Na_2O$ (wt. %)
SiO_2 (wt. %)
Macdonald hotspot:
Macdonald
Marotiri
Rapa
Raivavae
Rurutu (old)
Tubuai
Mangaia
Rimatara
Raratonga group:
Rarotonga Is.
Aitutaki
Arago hotspot:
Atiu
Rurutu (young)
Arago
Mauke
Aitutaki (old)
This study:
Rose atoll
Dino
Moki
Malulu
Papatua

Figure S3

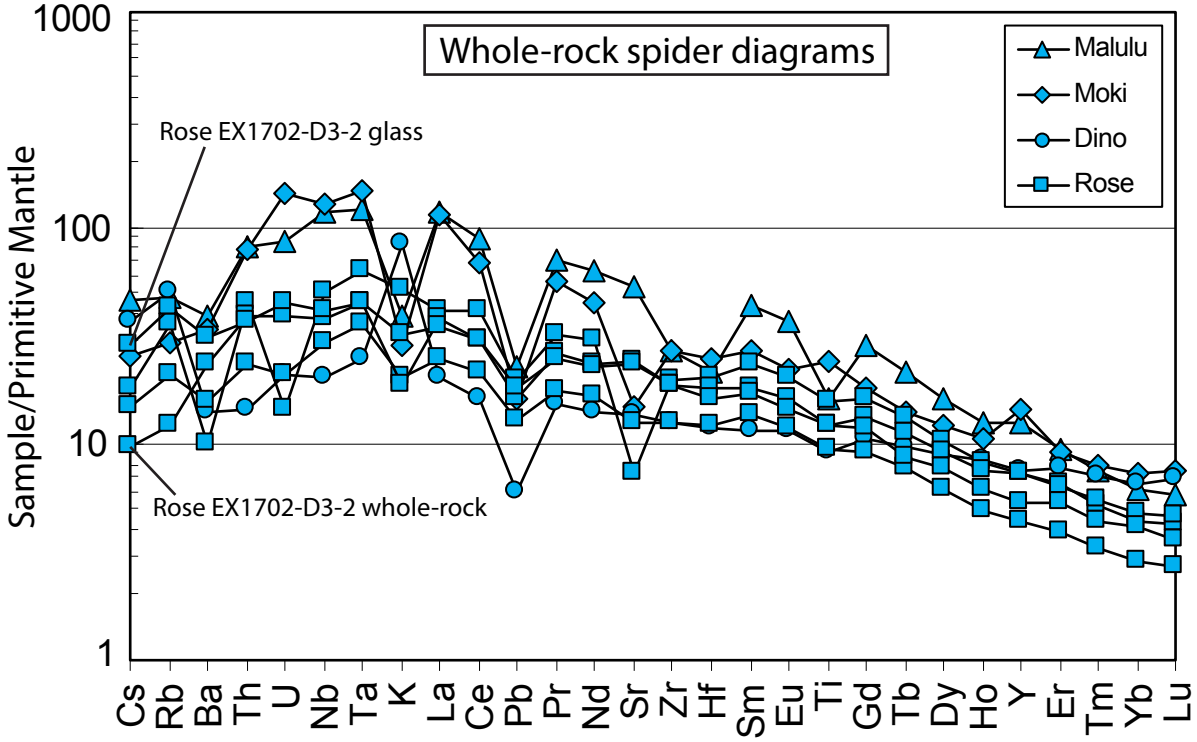
Whole-rock spider diagrams
Malulu
Moki
Dino
Rose
Rose EX1702-D3-2 glass
Rose EX1702-D3-2 whole-rock
Sample/Primitive Mantle
1000
100
10
1
Cs Rb Ba Th U Nb Ta K La Ce Pb Pr Nd Sr Zr Hf Sm Eu Ti Gd Tb Dy Ho Y Er Tm Yb Lu

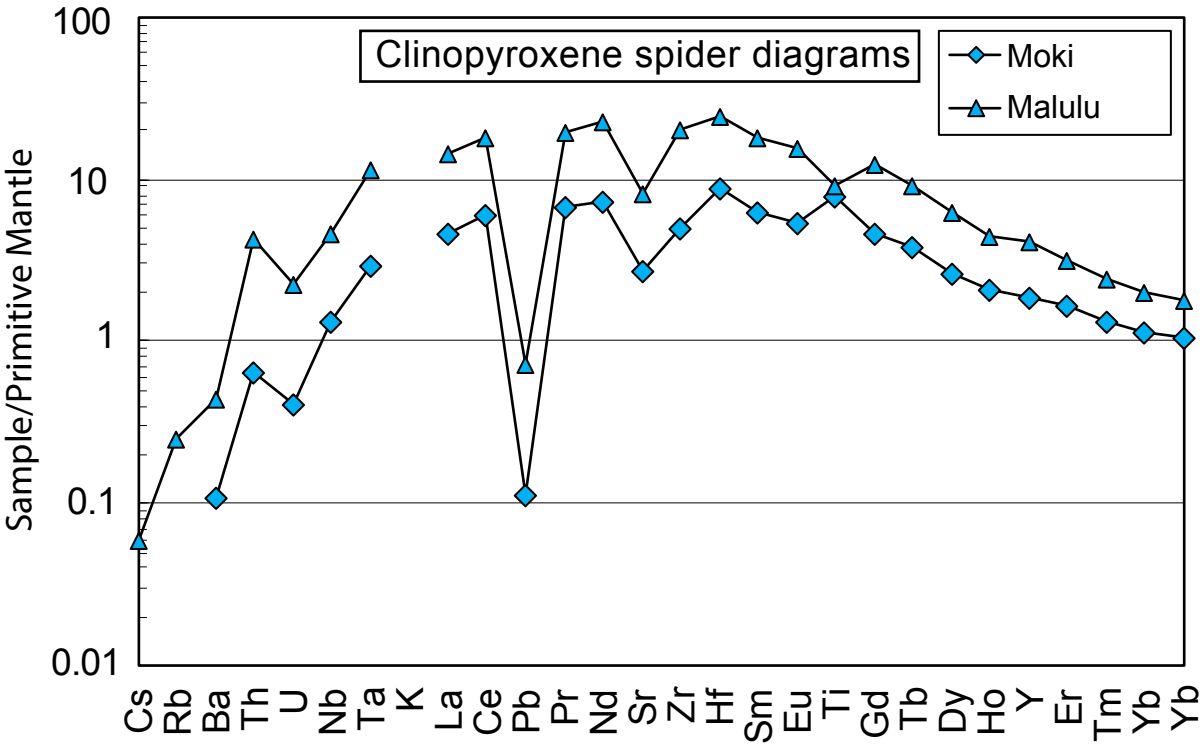
Clinopyroxene spider diagrams
Moki
Malulu
Sample/Primitive Mantle
100
10
1
0.1
0.01
Cs Rb Ba Th U Nb Ta K La Ce Pb Pr Nd Sr Zr Hf Sm Eu Ti Gd Tb Dy Ho Y Er Tm Yb Yb

Figure S4